Batteries & Supercaps

Review
doi.org/10.1002/batt.202200263

Chemistry Europe
European Chemical Societies Publishing

www.batteries-supercaps.org

Boron–Based Electrolytes for Rechargeable Magnesium Batteries: Biography and Perspective

Wen Ren,[a] Mingxiang Cheng,[a] Yaru Wang,[a] Duo Zhang,[a] Yang Yang,[a] Jun Yang,[a] Jiulin Wang,[a] and Yanna NuLi*[a]

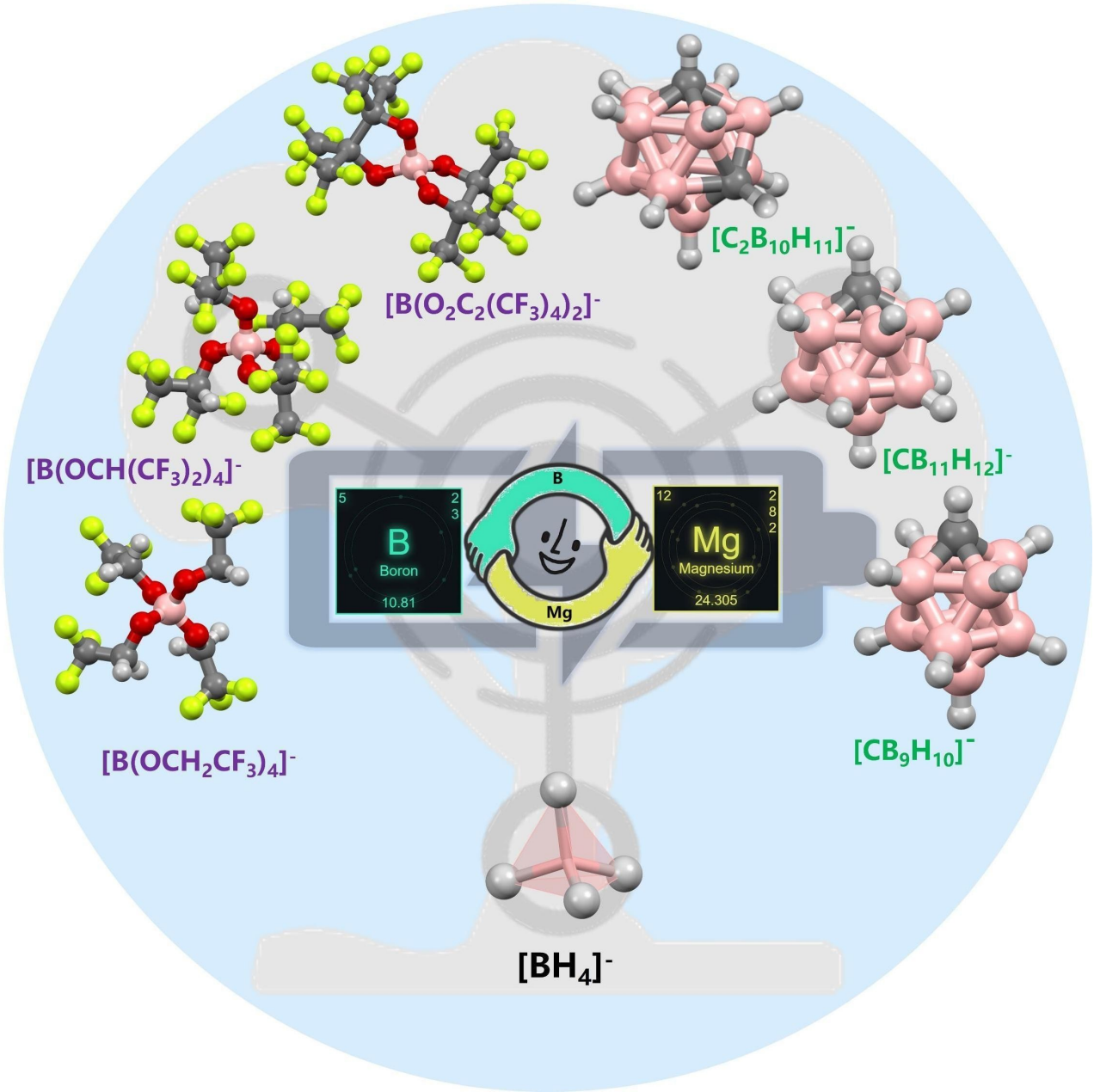

Rechargeable magnesium batteries (RMBs) are a promising alternative in the post–lithium era for their high volumetric capacity, crustal abundance, and metallic safety. Electrolytes for RMBs have experienced a development process from the initial Grignard compound to today's diversified single magnesium salt. Among them, the boron-based electrolyte plays a significant connecting link between the preceding and the following. This review retrospectively combed the origin and development course of boron–magnesium electrolyte and focuses on the application of three representatives: borohydride, boron-center fluorinated alkoxylate, and closo–borane cluster. Fundamental understandings and typical concerns correlative with the Mg–B electrolyte designs are highlighted and briefly discussed. Finally, future direction and possible proposals for practical Mg–B electrolytes are put forward.

1. Introduction

Aiming at alleviating the growing environmental crisis and tremendous pressure from fossil energy depletion, the global dedication to carbon peaking and neutrality has intensified the rapid R&D of sustainable energy technology. The solution of electrochemical energy storage (EES) satisfies the superiority of capacity, portability, and reliability simultaneously.[1] As the most influential representative, lithium-ion batteries achieved extensive commercial applications and greatly shaped our modern society. However, the development of lithium batteries has also encountered bottlenecks so far. Uneven geographical distribution of raw elements (e.g., Li, Ni, Co), price fluctuations vulnerable to geopolitics or artificial factors, especially, the intractable dendrite issue of highly–active metallic lithium, have greatly called for the next–generation post–lithium-ion battery technologies.[2] Hence, more research has focused on alternative monovalent (Na^+, K^+) or multivalent (Mg^{2+}, Zn^{2+}, Ca^{2+}, Al^{3+}) ions and made remarkable progress. As shown in Figure 1(a), parameters including specific/volumetric capacity, ionic charge density, and crustal abundance become comprehensive indicators to evaluate these energy storage strategies.[3]

Among them, magnesium has attracted considerable attention because of its moderate volumetric capacity (3833 mAh cm^{-3}), relatively low redox potentials (−2.36 V *vs.* SHE), and ideal abundance (2.1% crustal reserves, the sixth abundant metal element).[4] Meanwhile, another important advantage of rechargeable magnesium batteries (RMBs) is the extremely rare dendrite phenomenon in the process of repeated anodic electrochemical plating/stripping (Figure 1b). Although sporadic Mg dendrites have recently been reported in Grignard–based electrolytes, their extraordinary Mg plating current density and Grignard-restricted precondition (e.g., 10 mA cm^{-2} in 0.4 M all–phenyl complex (APC),[5] and 0.921 mA cm^{-2} in 0.5 M MeMgCl/THF[6]) may not obscure the comparable "dendrite–free" virtues of metallic Mg. The plating morphologies have also been proved a comprehensive function of current density, salt concentration, and additive of coordinating ligands.[7] Theoretically, the relevant DFT calculation demonstrated a lower self–diffusion energy barrier of metallic Mg(0001), which is 1/7 times (0.018 eV *vs.* 0.14 eV) that of Li(100).[8] This also explains why Mg electrodeposits tend to be bulky particles rather than needle–like morphologies.

Electrolytes that support the stable operation of RMBs are considered to require: 1) appropriate ionic conductivity and solubility to magnesium salts; 2) chemical inertness to reductive metallic Mg; 3) high electrochemical stability within the voltage window during the charging–discharging process. Unfortunately, the conventional electrolyte design strategy that dissolves simple salts in aprotic nonaqueous solvents (e.g., alkyl carbonate, esters, acetonitrile, and dimethyl formamide) w-as generally found to be incompatible with Mg metal, where the spontaneous passivation by–products formed at the anode/electrolyte interface insulated the Mg^{2+} and electrons simultaneously.[9] Even worse, the higher charge density of divalent Mg^{2+} (close ion radius but double positive charge *vs.* Li^+) further intensified the interaction force and de–solvation barrier. Whereas the Grignard reagent, a common Lewis base consisting of organo–magnesium (R–MgX, R = alkyl, X = halide) solutes and ether solvents, has attracted the attention by its fragile C–Mg bond and highly active nucleophilic property. As the development course of RMBs' electrolytes shown in Figure 1(c), the electrolysis research on Grignard reagents in the early 1920s indeed demonstrated acceptable reversibility of Mg plating/stripping. Compared with inorganic salts such as $MgCl_2$, $Mg(SO_3CF_3)_2$, $MgSO_4$, and $Mg(ClO_4)_2$, these Grignard–type solutes demonstrate superiorities such as the desired solubility in ethereal solvents, inertness to reductive metallic Mg, and high reversibility of electrochemical plating/stripping. In 1990, Gregory et al. opened an avenue in pursuit of the organo-magnesium chloride complexes via the combination of Lewis acid (aluminum halides, AlX_3) and Lewis base (Grignard reagents).[10] This strategy was continued to be carried forward by Aurbach et al. with the proposal of far–reaching DCC[11] (di–chloro complex, or 1st generation Mg electrolyte) and APC[12] (all phenyl complex, or 2nd generation Mg electrolyte). Although the electrochemical reversibility (~100% Coulombic efficiency (abbreviated as CE below)) and ionic conductivity (2–5 mS cm^{-1}) of these two organohaloaluminate electrolytes look promising, their complex active cation/anion species and limited oxidative stabilities seem inadequate in the demand for high–voltage cathodes.[13] Above all, the in-situ species generated by the Lewis acid/base combination are intrinsically nucleophilic, and therefore are incompatible with electrophilic cathodes (e.g., sulfur, selenium). Since 2010, the research of Mg electrolytes

[a] W. Ren, M. Cheng, Y. Wang, D. Zhang, Dr. Y. Yang, Prof. J. Yang, Prof. J. Wang, Prof. Y. NuLi
School of Chemistry and Chemical Engineering
Shanghai Jiao Tong University
800 Dongchuan Road, 200240 Shanghai, P. R. China
E-mail: nlyn@sjtu.edu.cn

Review
doi.org/10.1002/batt.202200263
Chemistry Europe
European Chemical Societies Publishing

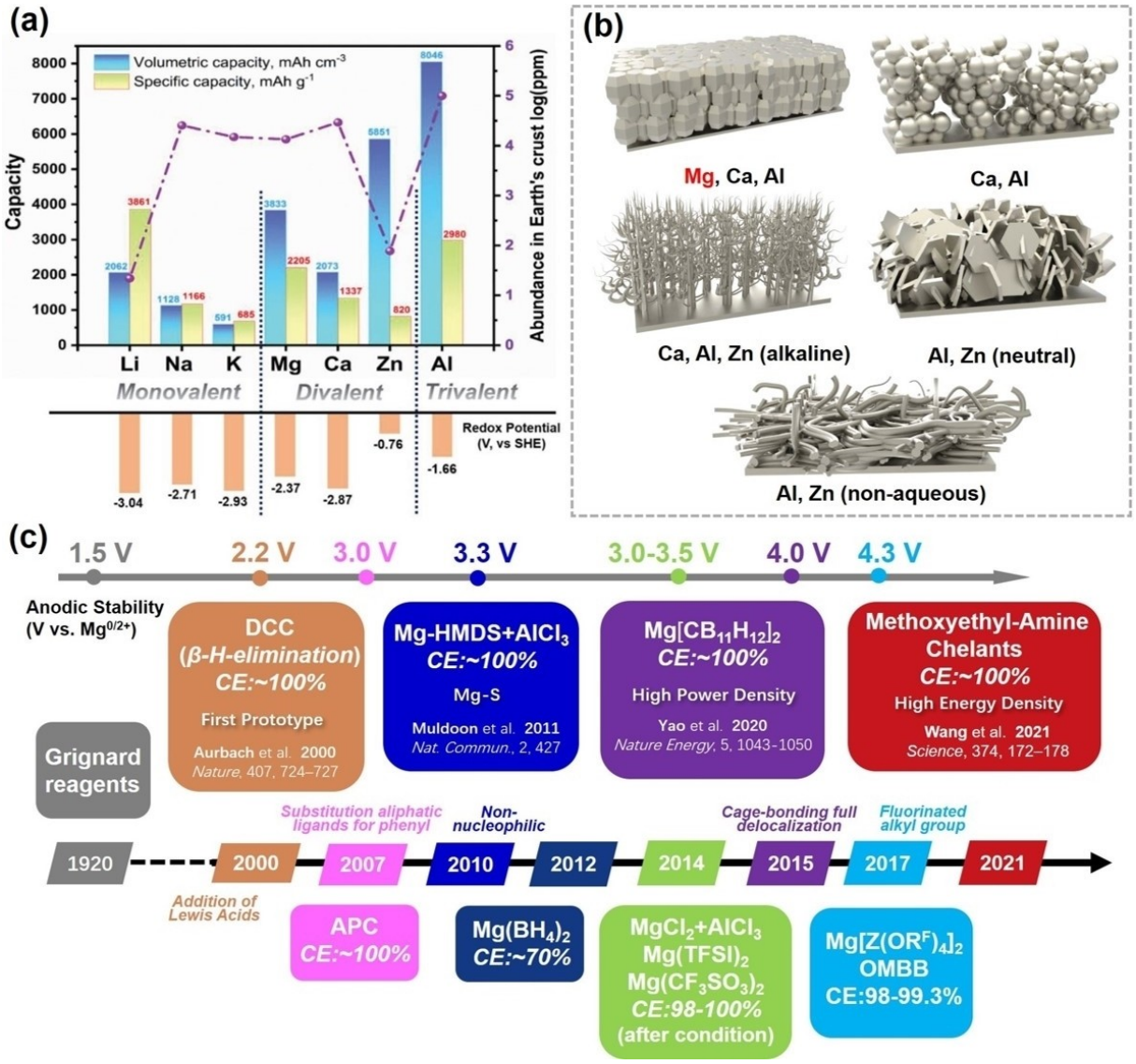

Figure 1. a) Capacities, abundance, and redox potential of various metal anodes for rechargeable batteries. Reprinted from Ref. [3b] with permission. Copyright (2022) Wiley-VCH. b) Typical plating morphologies of multivalent metal–ion metals. Reprinted from Ref. [23] with permission. Copyright (2020) Springer Nature. c) Development course of RMBs' electrolytes and corresponding milestone applications.

has been in a new stage dedicated to a non-Grignard reagent. Various non-nucleophilic Mg salts such as $Mg(HMDS)_2$,[14] $Mg(TFSI)_2$,[15] $Mg(CF_3SO_3)_2$,[16] and $MgCl_2$[17] have been thoroughly studied in the past decade. However, due to the more or less passivation effect of these anions to the Mg anode and thus unacceptable overpotential of plating/stripping, these electrolytes could not completely avoid the use of Cl^- ($AlCl_3$ or $MgCl_2$) which serves as an activator to adjust the Mg–electrolyte interface.[18] The chloride has been demonstrated to corrode normal current collectors and leads to the failure of the cell in

Wen Ren received his master's degree under the supervision of Prof. Yanna NuLi from Shanghai Jiao Tong University (SJTU) in 2022. Before studying at SJTU, he received his bachelor's degree from Nanjing Tech University in 2019. His research direction is advanced electrolytes for practical rechargeable magnesium batteries.

Prof. Yanna NuLi received her Ph.D. degree from Fudan University in 2001. After completing her postdoctoral research at Fudan, she joined Shanghai Jiao Tong University in 2003. Her main research interests focus on rechargeable magnesium batteries with high energy densities, including Mg–S, Mg–air, aqueous Mg–ion batteries, and Mg^{2+}–Li^+ hybrid batteries.

the long term.[19] The latest report claimed that highly reversible Mg plating/stripping could also be obtained by the strategy of solvation sheath reorganization in $TFSI^-$-based electrolyte, but the additive of methoxyethyl amine chelants on solid electrolyte interphase (SEI) formation and its wider cathode compatibility need to be further studied.[20]

Therefore, the research of Mg electrolytes has gradually entered the third stage: the single Mg salt solute with a bulky weakly coordinated anion (WCA), where B-based anion began to replace the Al–based as the protagonist of this generation of electrolytes. Actually, the boron, which is in the same IIIA group and possesses extremely similar chemical properties to Al, has also intrigued researchers' interest at a very early time. From the earliest alkyl/aryl substituted B-centered anions (e.g., $[BPh_xBu_{4-x}]^-$,[10,21] $[B(Ar^F)_4]^-$,[21] $[BPhMes_3]^-$[22]) to the fluorinated bulky alkoxyborate anions, the oxidative stability and weak coordination effect of anions have made a qualitative leap. As the classification shown in Figure 2, the boron–based electrolyte for RMBs could be divided into three main types according to their anions: (1) $[B–R_4]^-$, borohydride anions and its H-substitute derivatives; (2) $[B(OR^F)_4]^-$, fluorinated alkoxyl boron-centered anions; (3) $[C_xB_{12-x}H_{(12-x+1)}]^-$ (icosahedral) or $[C_xB_{10-x}H_{(10-x+1)}]^-$ (hexadecahedral) *closo*–carborane cluster anions.

This review is aimed at the latest retrospect of three representative Mg–B electrolytes with particular anions: borohydride and derivatives, fluorinated alkoxyl boron–centered anions, and *closo*-borane cluster anions. Synthetic route design and anode/cathode–electrolyte interface issues are highlighted, respectively. Meanwhile, several specific issues which have not been agreed upon in the Mg–B electrolytes are reconsidered.

2. Borohydride Anions and Derivatives

2.1. Magnesium borohydride

As one of the promising candidates for advanced hydrogen storage materials, magnesium borohydride has a high hydrogen capacity (14.9 wt%), low hydrogen–release temperature, and a small enthalpy change [41 kJ $(mol\ H_2)^{-1}$].[24] In 1957, Connor et al. first observed the impressive electrochemical Mg

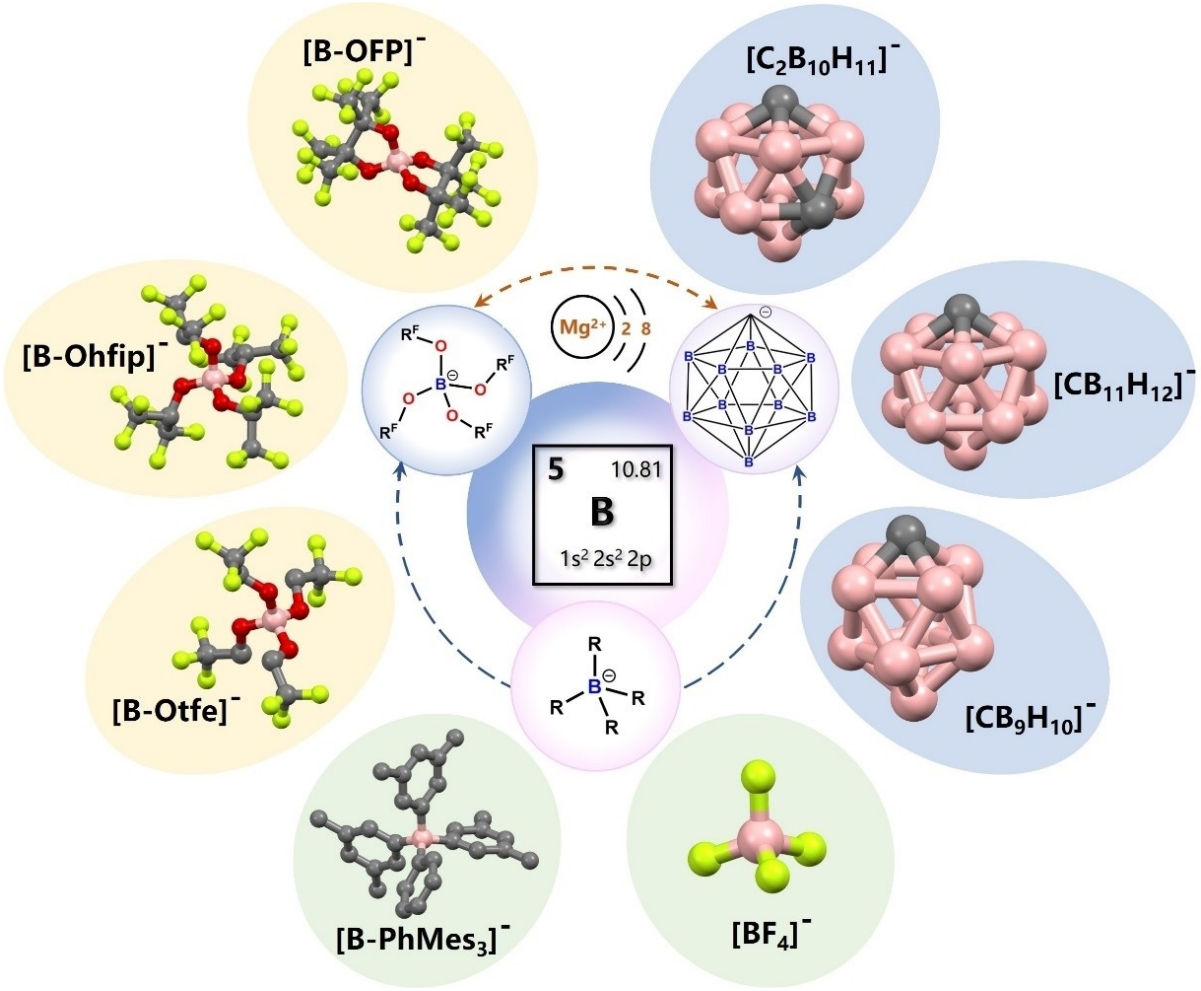

Figure 2. Classification of Mg–B electrolytes. R = alkyl, aryl, or halogen. R^F = fluorinated alkyl. Abbreviations of functional group are: OFP = fluorinated pinacolato, tfe = tri–fluoro–ethyl, hfip = hexa–fluoro–iso–propyl, Ph = phenyl, Mes = dimethylphenyl. Hydrogen atoms are omitted in the diagrams for clarity.

plating from the $Mg(BH_4)_2$/ether solutions.[25] Since the $[BH_4]^-$ is a strong reducing reagent, the strong ionic bond between Mg^{2+} and $[BH_4]^-$ leads to poor solubility in most ether solvents (~0.01 M), resulting in limited ionic conductivity (< 0.1 mS cm^{-1})[26] Although the deposit is not pure Mg and contained ~10 wt% co–deposit boron, the $Mg(BH_4)_2$ began to serve as a formal Mg salt solute and directly dissolved in ethereal solvents in later research.

2.1.1. Solute

In 2012, Mohtadi et al. first proved the reversible electrochemical Mg plating/stripping in the $Mg(BH_4)_2$/DME electrolyte, which opened the door for designing a new generation of B-based single salt electrolytes.[27] They also found the addition of $LiBH_4$ could significantly increase the current density (two orders of magnitude) and CE (from 70% to 94%) of Mg plating/stripping. This Mg–Li hybrid strategy is firstly applied to $[BH_4]^-$-based electrolyte, and the experimental evidence was inclined that $LiBH_4$ has a positive role in increasing $Mg(BH_4)_2$ dissociation of Mg^{2+} and $[BH_4]^-$. Shao et al. developed an optimized $Mg(BH_4)_2$–$LiBH_4$/DG (diglyme) electrolyte with 100% CE and 3.27 mS cm^{-1} ionic conductivity.[28] The increased ligand concentration of $[BH_4]^-$ from the $LiBH_4$ additive could accelerate the kinetics of the anodic Mg stripping process. NuLi et al. further reported the $Mg(BH_4)_2$–$LiBH_4$/TG (tetra-glyme) electrolyte with 95% CE and conductivity of 38 μS cm^{-1}.[29] Interestingly, the change of the glyme solvent slightly increased the oxidation stability from 2.2 V (DG, *vs.* Mg, on SS) to 2.4 V (TG, *vs.* Mg, on SS) but minified the ionic conductivity by about 100 orders of magnitude, which implies the significance of the solvent in $[BH_4]^-$-based electrolytes. The ionic liquid of 1-butyl-1-methylpiperidinium bis(trifluoromethyl sulfonyl) imide ($PP_{14}TFSI$) with high oxidation stability and reduction stability to Mg metal was introduced to the $Mg(BH_4)_2$–$LiBH_4$ electrolyte by NuLi et al.[30] The hybrid TG-DME-$PP_{14}TFSI$ solvent was reported a significantly improved conductivity (3.01 mS cm^{-1}) and oxidative stability (3.0 V *vs.* Mg, on SS).

2.1.2. Anode interface activator

Electron-rich $[BH_4]^-$ anion is regarded as one of the few anions permitting reversible Mg plating/stripping without halogen. Due to its strong base property and propensity to be oxidized, $[BH_4]^-$ anion demonstrated impressive chemical stability against reductive metallic Mg.[31] Recently, researchers deeply reexplored the multiple functions of $[BH_4]^-$ as the development of advanced characterization technology. More research have revealed that the $[BH_4]^-$ additive also plays a positive role to activate the Mg anode interface in electrolytes such as bis(trifluoromethane)sulfonylimide ($TFSI^-$),[32] hexa-methyl-disilazide ($HMDS^-$),[33] and tetrakis(hexa-fluoro-iso-propyloxy) borate ([B-(Ohfip)$_4$]$^-$).[34] In the $TFSI^-$ system, Shao et al. suggested that the $[BH_4]^-$ was able to participate in the coordination of $[Mg\cdot 2DG–TFSI]^+$ solvation sheath and form neutralized $[Mg\cdot DG–TFSI–(BH_4)]$ cation cluster, thus mitigate the decomposition of $TFSI^-$.[35] Meanwhile, the preferential absorption of $[BH_4]^-$ on the Mg surface can repel the $TFSI^-$ away from Mg and suppress its further reduction. In the $HMDS^-$ system, Seh et al. proposed a $[BH_4]^-$-based additive to prevent the Mg anode passivation, as long as 20 mM additives could enhance the initial CE of the Mg plating from 64.8% to 74.2% and reduce the overpotential from −1.4 V to −0.7 V.[33] They suggested that the $[BH_4]^-$ served as the moisture scavengers by chemically reducing the H_2O or other protic contaminants. Surface analysis of the Mg anode reveals the formation of a robust SEI at the anode–electrolyte nanointerface, which allows magnesium plating/stripping to occur reversibly.

In the $Mg[B(Ohfip)_4]_2$ electrolyte, the $Mg(BH_4)_2$ is also able to reduce the conditioning period of $Mg[B(Ohfip)_4]_2$/DME electrolyte via removing the native oxide layer and reconstructing Mg^{2+} conductive SEI.[34] In Figure 3(a–d), the plating of Mg^{2+} on Pt demonstrated a significant reduction of initial overpotential in the $[BH_4]^-$ additive-containing electrolyte, accompanied by a more prominent CV response current and higher CEs in the following Mg plating/stripping process. The scheme of anode-interphase formation from the $[BH_4]^-$ anion is shown in Figure 3(e), Arthur et al. assumed that the contact-ion pair $[Mg(\mu\text{-}H)_2BH_2]^+$ is the active component in the process of anodic plating.[36] Through operando sXAS and TEM, they determined the decomposed product of boron cluster $[B_xH_y]^-$ and initial H_2-gas evolution in the formation of an SEI. Theoretical calculation of B–H bond dissociation energy (BDE) in Figure 3(f) demonstrates a decrease by 1.22 eV when the $[BH_4]^-$ anion is associated with a reduced, transient Mg^+.[37] The weakening B–H bond energy also verified the possibility of H dissociation from the central B atom. But the side effect of $[BH_4]^-$ additive is also obvious: the higher concentration of $[BH_4]^-$ would result in a loss of oxidative stability. This detrimental effect is related to the intrinsic inferior oxidative stability of $[BH_4]^-$. Thus, the modification of the function group on the $[BH_4]^-$ anion has become a significant starting point to enhance the oxidative stability of the $Mg(BH_4)_2$ family electrolyte.

2.2. Borohydride derivatives

$[BH_4]^-$ is the simplest B-centered anion, but it was not until 2012 that Mohtadi et al. first verified a surprising Mg plating/stripping reversibility (67% CE) of the $Mg(BH_4)_2$/DME electrolyte.[27] Although this simple $Mg(BH_4)_2$/ether electrolyte demonstrated certain electrochemical properties, its oxidation onset potential is too low (1.7 V *vs.* Mg on Pt) to be practically utilized for high voltage RMBs. In line with the demand for an improving oxidative stability, the logic modification would be mainly divided into two directions: 1) incorporation of electron-withdrawing groups such as $–CF_3$ and halogen atom with strong electronegativity; 2) increase the volume of B-centered anions. The strong attraction of fluorine toward electrons can restrain the electron loss at high voltage, meanwhile, bulky anions are beneficial to improving the salt solubility due to the

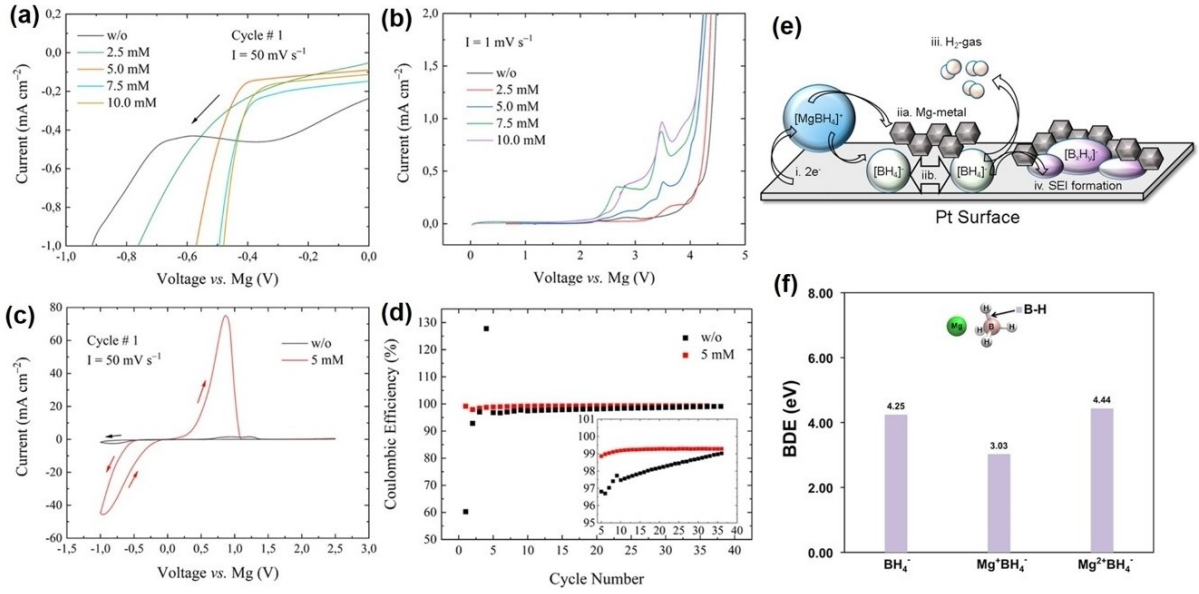

Figure 3. a) Initial CV of the $Mg[B(Ohfip)_4]_2$/DME electrolyte with/without the $Mg(BH_4)_2$ additive; b) LSV with various additive concentrations; c) initial CV with the neat electrolyte and with 5 mM $Mg(BH_4)_2$; d) Coulombic efficiency of Mg plating/stripping using the neat electrolyte and with 5 mM $Mg(BH_4)_2$. a)–d) Reprinted from Ref. [34] with permission. Copyright (2021) The Authors. Published by American Chemical Society. e) Interphase formation process in $Mg(BH_4)_2$ electrolytes. Reprinted from Ref. [36] with permission. Copyright (2017) American Chemical Society. f) Bond dissociation energy (BDE) of $[BH_4]^-$ anion corresponding to well-solvated, Mg^+-ion paired, and Mg^{2+}-ion paired. Reprinted from Ref. [37] with permission. Copyright (2015) American Chemical Society.

decreased lattice energies affected by increasing unit volume.[38]

Despite improved oxidation stability, the tetrahedral $[BF_4]^-$ anion has been experimentally proved to passivate the Mg-metal anode.[10,39] The failure of $[BF_4]^-$ inspires the combination of fluorination and moderate increase of anion volume, this "bilateral" strategy has been developed in the following fluorinated alkoxyl organoborate electrolytes. On the other hand, the researchers were in an attempt to form bulky anions by introducing the electrons-conjugated alkyl/aryl groups to the central B-atom. In 2012, Yang et al. proposed the electrolytes based on $[B(PhMes_3)]^-$ anion and extend the oxidation onset potential to 3.5 V *vs.* Mg on Pt.[22] Muldoon et al. then proposed the chloride-free electrolyte based on $[B(Ph)_4]^-$ anion.[21] Their result indicated that magnesium organoborates are non-corrosive in nature at high voltages and provided a crucial reference for the development of B-based electrolytes afterward. The property comparison of anodic Mg plating/stripping in $[BH_4]^-$-based and derivative electrolytes are summarized in Table 1.

3. Fluorinated Boron–Centered Anions

The magnesium fluorinated alkoxyl organoborates, or $Mg[B(OR^F)_4]_2$, is a significant WCA-based electrolyte in Mg batteries. The bulky $[B(OR^F)_4]^-$ anion consists of a characteristic central B atom and four fluoroalkoxy branched chains. These fluorine groups at the ends of the four branched chains possess a strong electron-absorbing effect, which avoids the excessive concentration of the electron cloud around the central B atom, that is, the negative charge tends to be uniformly distributed to the surface layer of $[B(OR^F)_4]^-$ anion.[45] The larger volume of the $[B(OR^F)_4]^-$ anion also poses a positive role to weaken the charge density. The identical structure of four peripheric branched chains and the four–even coordination number of B bring a symmetrical charge distribution. Therefore, the divalent Mg^{2+} cation is almost coordinated by the solvent molecules, the relatively independent cation/anion brings a weaker interaction in comparison with other small anions.

3.1. Comparison of synthetic routes

The $Mg[B(OR^F)_4]_2$ originated from the fluorinated functional group substitution toward the H atoms of $[BH_4]^-$ and could be commonly synthesized by two different routes (Figure 4). Zhao-Karger et al. have made a pioneering contribution to the synthesis of $Mg[B(OR^F)_4]_2$ and opened an avenue via the single-step dehydrogenation reaction between the commercial $Mg(BH_4)_2$ and fluorinated alkyl alcohols ($H–OR^F$). Under this framework, they first proposed the $Mg[B(Ohfip)_4]_2$) electrolyte through the reaction between $Mg(BH_4)_2$ and hexafluoroiso–propanol (hfip–OH). As the Route I showed in Figure 4(a), the OR^F group is directly derived from fluoroalchols, so the selection of different alcohol precursors is a significant way to design and regulate B-based anions with various structures. Liu et al. chose the perfluoropinacol as the $H–OR^F$ and synthesized the $Mg[B(OFP)_2]_2$ electrolyte.[46] The bidentate alkyloxide ligands in the –OFP group form a connected ring structure, which brings a unique chemical stabilization and tolerance to moisture/oxygen. The reported $Mg[B(OFP)_2]_2$/TG electrolyte showed an Mg plating/stripping overpotential as low as 0.197 V and oxidative stability reaching 4.0 V (*vs.* Mg, on SS).

Table 1. Property comparison of anodic Mg plating/stripping in $[BH_4]^-$-based electrolytes.

Electrolyte		Concentration[a] [M]	Ionic conductivity [mS cm^{-1}]	Coulombic efficiency	Oxidative stability [V] (substrate)	Mg stripping current density [mA cm^{-2}]	Ref.
$Mg(BH_4)_2$	/THF	0.5	–	40 %	1.7 (Pt) 2.2 (SS)	0.032	[27]
	/DME	0.1	–	67 %	1.7 (Pt)	0.25	[27]
	/DG	0.01	–	77 %	~1.7 (Pt)	0.05	[40]
	/TG	0.01	–	84 %	~1.7 (Pt)	0.3	[40]
	/$MPEG_7PyrTFSI$	0.5	0.24	90 %	2.0 (Pt)	2	[41]
	0.6 M $LiBH_4$/DME	0.18	–	94 %	1.7 (Pt)	25	[27]
	1.5 M $LiBH_4$/DG	0.1	3.27	99 %	1.9 (Pt)	12.5	[28]
	1.5 M $LiBH_4$/TG	0.5	9.66	100 %	2.0 (Pt)	4	[29]
	0.25 M $LiBH_4$/$PP_{14}TFSI$-TG-DME (2 : 1 : 1, v/v)	0.25	3.01	92 %	3.0 (SS)	10	[30]
$Mg(BR_4)_2$	$Mg(BBu_2Ph_2)_2$/THF	0.4	1.79	50 %	2.5 (Pt)	2.6	[42]
	$Mg(BMes_3Ph)_2$/THF	0.25	1.5	100 %	2.6 (SS)	3.8	[43]
	$Mg(BAr^F)_2$/THF	0.05	1.5	–	4.0 (SS)	–	[21]
	2 PhMgCl–$BMes_3$/THF	0.5	2	100 %	3.5 (Pt)	9	[22]
	0.5 $Mg(Bu)_2$–BCl_3/THF	0.25	–	93 %	1.75 (Au)	0.9	[44]
	1.5 $Mg(Bu)_2$–BPh_3/THF	0.25	–	86 %	1.77 (Au)	0.2	[44]
	$[Mg_2Cl_3\ 6THF][BPh_4]$/THF	0.2	–	–	2.6 (SS)	–	[21]
	$[Mg_2Cl_3\ 6THF][B(C_6F_5)_3Ph]$/THF	0.2	–	–	2.2 (SS)	–	[21]

[a] the concentration of Mg^{2+}, M = mol L^{-1}.

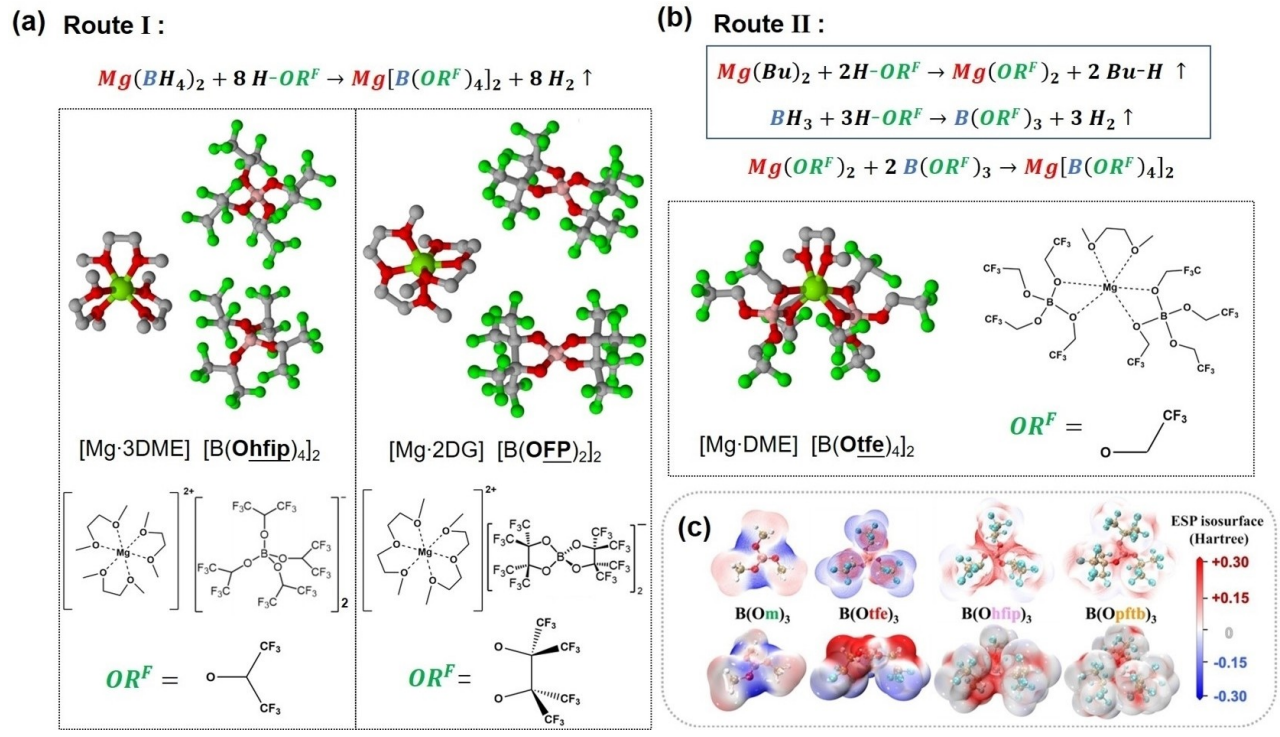

Figure 4. a), b) Two common routes for the synthesis of fluorinated alkoxyl borate electrolytes. c) Electrostatic potential (ESP) iso-surface of $B(OR)_3$ borates with different degrees of $-CF_3$ group substitution. Reprinted from Ref. [51] with permission. Copyright (2021) American Chemical Society.

On the other hand, Mandai et al. proposed Route II which separated the Mg and B from the single $Mg(BH_4)_2$ salt and replaced them with $Mg(Bu)_2$ and BH_3, respectively.[47] Through the transmetalation reaction between $Mg(OR^F)_2$ and $B(OR^F)_3$, the same $Mg[B(OR^F)_4]_2$ structure would be obtained by a step-by-step route. Despite the introduction of more complicated steps, the Mg plating/stripping current density of the $Mg[B(Ohfip)_4]_2$ electrolyte synthesized from Route II is three times higher than that of Route I. In view of the unstable yield reproducibility, hard source availability, and operation difficulty of the $Mg(BH_4)_2$, the significance of this work is not only paved a facile and reliable avenue for the synthesis of $Mg[B(OR^F)_4]_2$

but also greatly reduces the cost of the raw materials by ~74%. Fortunately, the intermediate product $B(OR^F)_3$ borate from the second step in Route II is commercially available, providing another simplified route that uses the in-situ reaction between commercial $B(OR^F)_3$ borate and various Mg salts. In fact, the Cui group has made a systematic study on this in-situ reaction strategy. They used the common inorganic magnesium salt ($MgCl_2$,[48] MgF_2,[49] and MgO[50]) as the Mg source to directly react with the $B(Ohfip)_3$ borate. Among them, the salt sources of $MgCl_2$ (OMBB) and MgF_2 (BCM) demonstrate wide compatibility with various cathode materials as summarized in Table 2.

In the $Mg[B(OR^F)_4]_2$ electrolyte, an important issue is how to evaluate the effect of fluorination degree on the $[B(OR^F)_4]^-$ anions and following electrochemical performances. As shown in Figure 4(c), NuLi et al. studied the electrostatic potential (ESP) iso–surface change as the deepening of fluorination degree, the positive and negative charge centers of $B(OR^F)_3$ molecular are no longer concentrated on a particular atom but tend to be conjugated.[51] When weaker fluorinated trifluoroethanol (tfe-OH) was used as the alcohol precursor, the diluted regional charge polarization is further manifested, and thus the weakened coordination effect brings an incomplete dissociation of B-centered anion and Mg^{2+}. The synthesized $[Mg\cdot DME][B(Otfe)_4]_2$/THF ($B(Otfe)_4$ = tetra(trifluoroethyloxy) borate) electrolyte also showed an oxidation decomposition potential reaching 3.3 V (*vs.* Mg, on SS) and 96% CE of anodic Mg plating/stripping. Similarly, the in-situ route using commercial $B(Otfe)_3$ (tris(trifluoroethyl) borate) and $MgCl_2$ was carried out by Li et al.[52] The active tetracoordinated $[B(Otfe)_4]^-$ anion and $[Mg_2Cl_2\cdot 4DME]^{2+}$ cation cluster were detected by ESI-MS. This Cl-containing design also endows it with a favorable anodic overpotential and reversibility in Mg||Mg symmetric cell. NuLi et al. recently reported the similar $[Mg_2Cl_2\cdot 6THF]^{2+}$ structure in the $MgCl_2$-$2B(Otfe)_3$/THF electrolyte, the theoretical calculation also revealed a positive role of the chlorine-containing cation in lowering the de-solvation energy barrier and contributing a more favorable energy path of the magnesium plating process, especially compared with the chlorine-free MgF_2-$B(Otfe)_3$/DME electrolyte.[53]

3.2. Anode–electrolyte interfaces

The electrochemical characterization of the 0.3 M $Mg[B(Ohfip)_4]_2$/DME electrolyte is showed in Figure 5(a–f). Oxidation stability up to 4.8 V *vs.* Mg, ionic conductivity above 10 mS cm^{-1}, and Mg plating/stripping overpotential less than 0.1 V, these competitive indicators highlight the $Mg[B(Ohfip)_4]_2$

Table 2. Property comparison of the $Mg[B(OR^F)_4]_2$ electrolytes and their cathode compatibility.

Electrolyte	Ionic conductivity/ [mS cm^{-1}] (Concentration)	Coulombic efficiency	Oxidative stability [V] (substrate)	Cathode	Capacity [mAh g^{-1}] @ current density [mA g^{-1}] (cycle)	Ref.
$Mg[B(Ohfip)_4]_2$/DME	6.8 (0.6 M)	98%	4.3 (SS) 3.5 (Pt)	S-CMK3	200 @ 0.1 C[a] (100)	[53b]
				S-ACC	320 @ 0.1 C[a] (60)	[59]
				S-NC	228 @ 0.02 C[a] (50)	[63]
				S-$Ti_3C_2T_x$/CNT	450 @ 50 (10)	[64]
				VS_4/rGO	200 @ 100 (50)	[65]
				TiS_2	50 @ 20 (30)	[66]
				CuS-CTAB2	111 @ 560 (1000)	[67]
				14PAQ@KB	50 @ 2 C[b] (2000)	[68]
				CuDEPP	72 @ 4000 (500)	[69]
$B(Ohfip)_3$–MgF_2/DME (also denoted as **BCM**)	1.1 (0.05 M)	99%	3.5 (SS)	S/C (acetylene black)	934 @ 50 (30)	[49]
				Se-Cu	280 @10 (100)	[70]
				$Cu_{2-x}Se$	140 @ 100 (250)	[71]
				Cu_3Se_2	250 @100 (400)	[72]
				Te-Cu	332 @100 (50)	[73]
$B(Ohfip)_3$–$MgCl_2$–Mg/DME (also denoted as **OMBB**)	5.58 (0.5 M)	98%	2.5 (SS) 3.3 (Pt)	Mo_6S_8	50 @ 200 (1200)	[48]
				S-CNT	1019 @160 (100)	[48]
				SeS_2/CMK3	299 @ 3 C[c] (1000)	[74]
$B(Ohfip)_3$–$Mg(BH_4)_2$/DG	3.72 (0.5 M)	99%	2.8 (SS)	Mo_6S_8	72 @ 30 (600)	[26b]
				S/C (disordered mesoporous)	526 @ 50 (30)	[26b]
$B(Ohfip)_3$–MgO/DME	0.174 (0.0485 M)	–	4.2 (SS)	Mo_6S_8	45 @ 45 (400)	[50]
				S	900 @10 (6)	[50]
$Mg[B(Otfe)_4]_2$/THF	0.4 (0.75 M)	96%	3.3 (SS)	Mo_6S_8	57 @ 0.05 C[d] (210)	[51]
$B(Otfe)_3$–MBA/THF	–	98%	2.8 (SS)	Cu_3Se_2	61 @10 (200)	[51]
$B(Otfe)_3$–$MgCl_2$–$CrCl_3$–Mg/DME	1.79 (0.25 M)	97%	2.7 (SS) 3.5 (Pt)	CuS	231 @ 56 (100)	[52]
$B(Otfe)_3$-MgF_2/DME	–	80%	3.0 (Pt)	Mo_6S_8	67 @ 0.05 C[d] (40)	[53]
$B(Otfe)_3$-$MgCl_2$/THF	–	93%	3.0 (Pt)	Mo_6S_8	60 @ 0.05 C [d] (40)	[53]
$Mg[B(OFP)_2]_2$/DG	3.95 (0.5 M)	95%	4.0 (SS)	MnO_2	150 @ 0.01 (1)	[46]
				PAQS/CNTs	64 @ 0.5 C[e] (100)	[75]

[a] S, 1 C = 1672 mAh g^{-1}. [b] 14PAQ@KB, 1 C = 260 mAh g^{-1}. [c] SeS_2/CMK3, 1 C = 1125 mAh g^{-1}. [d] Mo_6S_8,1 C = 128.8 mAh g^{-1}. [e] PAQS, 1 C = 225 mAh g^{-1}.

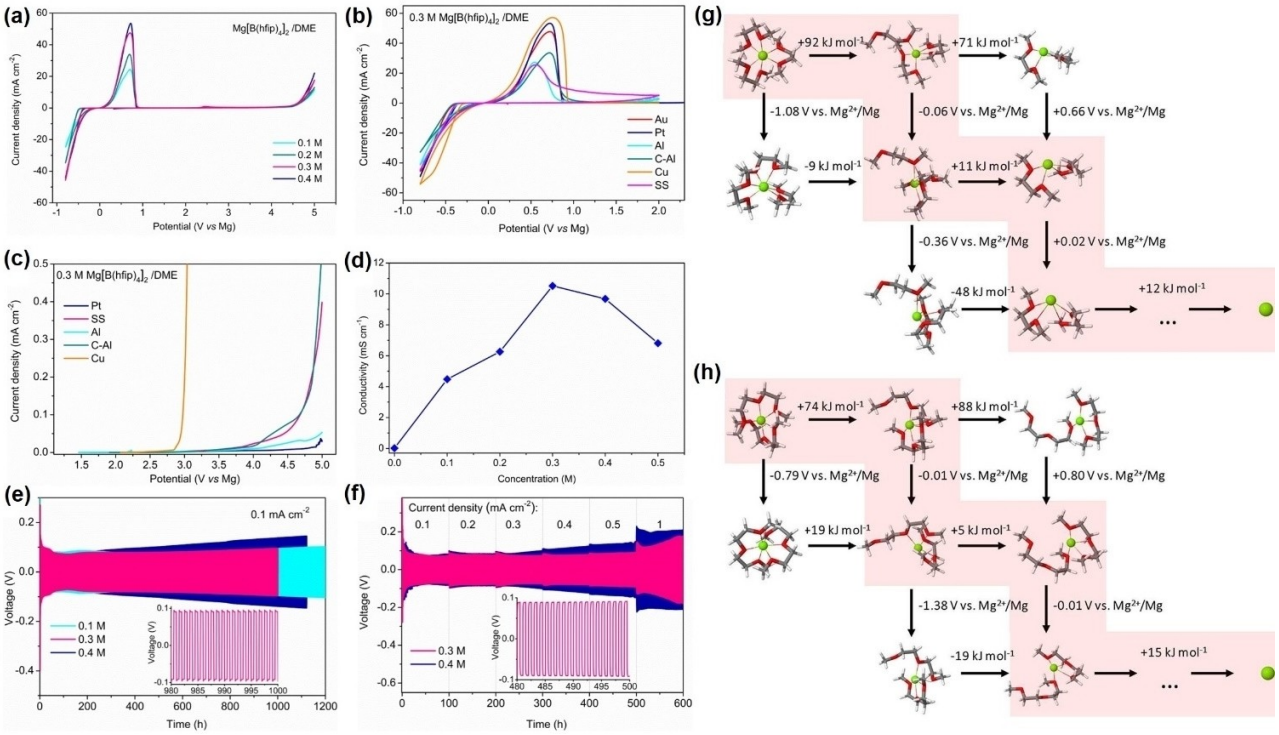

Figure 5. Electrochemical characterizations of the $Mg[B(Ohfip)_4]_2$/DME electrolyte: a) classification CVs on the Pt electrode; b) CVs and c) LSVs on different metal electrodes; d) conductivities at R.T; e) long-term Mg stripping/plating and f) cycling performance at various current densities. a)–f) Reprinted from Ref. [60] with permission. Copyright (2018) American Chemical Society. Possible de–solvation (horizontal) and reduction (vertical) processes for g) $[Mg{\cdot}3\,DME]^{2+}$ and h) $[Mg{\cdot}2\,DG]^{2+}$ in the $Mg[B(Ohfip)_4]_2$ electrolyte. g) and h) Reprinted from Ref. [59] with permission. Copyright (2021) The Authors. ChemSusChem published by Wiley-VCH GmbH.

among one of the best Mg electrolytes nowadays. However, the long-term cycling of the $Mg[B(Ohfip)_4]_2$ electrolyte was not as expected, owing to the formation of porous Mg deposits which penetrate the separator during cycling.[54] The porous structure indicated that the SEI generated in $Mg[B(Ohfip)_4]_2$ was not rigid enough to guide uniform Mg deposition.[47] Cui et al. reported a Mg-protection method via the decomposition of $Li[B(Ohfip)_4]$ additive, after which generates a stably hybrid Mg^{2+}/Li^+ SEI film (~0.5 kΩ *vs.* 20 kΩ prior to Li^+ incorporation) and thus circumvent the insufficient stability of $[B(Ohfip)_4]^-$.[54a] In contrast to the porous Mg deposited from the $Mg[B(Ohfip)_4]_2$ electrolyte, the $Li[B(Ohfip)_4]$ solution realized a more compact and uniform morphology.

Recently, metals with low alloy formation enthalpy of Mg (e.g., Ge, Sn, and their compounds) have been reported to protect the Mg anode.[55] In the $Mg[B(Ohfip)_4]_2$ system, Meng et al. investigated an additive of bismuth(III) trifluoromethanesulfonate ($Bi(OTf)_3$), the in-situ formed Bi/Mg_3Bi_2 film on the Mg surface would reduce the absorption of inactive species and thus enhance the resistance to passivation.[56] Parambath et al. reported the addition of optimum concentration of iodine additive, which helps in the formation of a favorable, less corrosive, uniform, and stable interfacial layer.[57] The large Mg plating/stripping overpotential in the presence of polysulfide species decreased significantly after the addition of optimum concentration of iodine, which also avoids the time-consuming electrolytic conditioning behavior. The formation of the MgI_2 protective layer on the Mg anode helps to reduce harmful side reactions while forming an electrochemically stable, thinner, and uniform Mg^{2+} conductive interface between the metallic Mg and the $Mg[B(Ohfip)_4]_2$ electrolyte.

Another significant concern in the anode-electrolyte interface is the specific de-solvation process of Mg^{2+} cations. The de-solvation usually goes along with high energy barriers, which can have a crucial impact on the plating reaction.[58] Drews et al. developed a kinetic model coupling the de-solvation to electron transfer at metal Mg anode.[59] They demonstrated that it is not necessary to peel the entire solvent molecule from the solvated magnesium cation before the first step of reduction. As shown in Figure 5(g and h), the $Mg[B(Ohfip)_4]_2$/DME and/DG demonstrate huge similarities in the de-solvation process. Firstly, a single coordination site (normally six sites) is desolvated from the octahedral Mg–O structure, after which the transfer of one electron reduces the charge of the Mg^{n+} cation (*n*: from 2 to 1). The energy required for the first step of desolvation is several times greater than that after electron transfer (92 *vs.* 11 kJ mol^{-1} for DME, 74 *vs.* 5 kJ mol^{-1} for DG). Thereby, the initial desolvation of the magnesium cation is the most crucial step and determines the kinetics of the entire Mg plating.

3.3. Cathode compatibility

As one of the most excellent Mg–B electrolytes, the compatibility of $Mg[B(OR^F)_4]_2$ electrolytes with various cathodes have been widely studied, including but not limited to electrophilic sulfur/selenium and Cu compounds, transition metal sulfides, and organic quinone-based polymers. Property comparison of these $Mg[B(OR^F)_4]_2$ electrolytes and their cathode compatibility are summarized in Table 2.

4. *Closo*–Carborane Cluster Anions

A remarkable feature of boron is that it is easy to form polyborane anion with multiple boron atoms. Besides the fluorination substitution to improve the oxidative stability and curb the hydridic reactive of $Mg(BH_4)_2$, another promising strategy is to establish a stable three-dimensional B–B bond structure as in the poly–boron cluster.[61] Due to the presence of tangentially delocalized sigma bonding in the boron framework, the three-dimensional $[B_nH_n]^{2-}$ ($n=6$–12) family contains two highly delocalized negative charges and is dispersed by the whole bulky cluster, making it possible for serving as a WCA toward divalent Mg^{2+}.[62] Among them, the representative dianion $[B_{12}H_{12}]^{2-}$ was first received attention and targeted as the potential electrolyte for RMBs for its attractive stability. However, the almost insolubility in ethers hampered its further electrochemical application, thus, researchers have proposed a [CH] substitution of [BH] to reduce the total cluster negative charge and therefore further weaken the charge density. Because the C atom is more electronegative than B, the radial bonds are typically polarized toward the C–H substituents.[63] C*loso*–carborane cluster anions $[C_xB_{12-x}H_{(12-x+1)}]^-$ (icosahedral) and $[C_xB_{10-x}H_{(10-x+1)}]^-$ (hexadecahedral) enjoy an even coordinator number and related symmetrically spatial stability, which has been reported for the first time in RMBs' electrolytes.

4.1. Comparison of synthetic routes

Mohtadi et al. have made a pioneering contribution in the application of this bulky *closo*–carborane anion. As shown in Figure 6(a), they first proposed the $Mg[C_2B_{10}H_{12}]_2$ electrolyte in 2014 through the substitution reaction between Grignard iPr–MgCl and the hydrogen of neutral m-carborane $C_2B_{10}H_{12}$.[39] The as-formed $C_2B_{10}H_{11}$–MgCl compound also possesses a conventional Schlenk equilibrium (Figure 6b) which is similar to the Grignard reagent. The formed $[(C_2B_{10}H_{11})_2MgCl]^-[Mg_2Cl_3]^+$/THF electrolyte demonstrated a highly reversible redox couple (98.2% CE, Figure 6c) of Mg plating/stripping and an anodic stability reaching 3.2 V (*vs.* Mg on Pt, Figure 6d). But this double C–H substitution and Cl containing strategy did not completely separate the $[C_2B_{10}H_{11}]^-$ anion from Mg^{2+}. Meanwhile, the corrosivity that arises from the halogen has not been eliminated.

Based on the deficiencies of the $[C_2B_{10}H_{11}]^-$ anion, Mohtadi et al. further reported a single C–H substituted $[CB_{11}H_{12}]^-$ anion in 2015.[77] As shown in Figure 7(c), they first proposed the AgBr precipitation method to synthesize pure $Mg(CB_{11}H_{12})_2$ salt. It should be mentioned that the Mg^{2+} is unassociated with the bulky carborate anion and completely solvated by TG/DG solvent due to the more weakly coordinating effect of $[CB_{11}H_{12}]^-$ anion in comparison with the dicarborate. The electrochemical performance of the $Mg(CB_{11}H_{12})_2$/TG electrolyte is shown in Figure 7(a, b), the as-synthesized magnesium monocarborane (MMC) salt/G4 electrolytes have a high solubility (>1 M), CE of >94.4% and oxidative stability up to 3.8 V (on Pt). In view of the high cost of the $Ag(CB_{11}H_{12})$ raw precursor, Lavallo et al. reported a precious metal free method to synthesize the same $Mg[CB_{11}H_{12}]_2$ salt from the reduction of the ammonium cation in $[HNMe_3]^+[CB_{11}H_{12}]^-$.[80] They further combined the as-synthesized $Mg[CB_{11}H_{12}]_2$ salt with $MgPh_2$, and the formed $[MgPh\cdot THF\cdot 2DME]^+$ was certified as the active cation cluster and 12.4 mS cm^{-1} was obtained in the electrolyte of $Mg[CB_{11}H_{12}]_2$–$MgPh_2$/DME (0.4 M). As shown in Figure 7(f, g), the remarkable oxidative stability is up to 4.2 V on Ti and 3.5 V on both SS and Ni, accompanied by an average CE of 95% in the following 50 cycles. The property comparison of the Mg–carborane cluster electrolytes and their cathode compatibility are summarized in Table 3.

4.2. Halogenation modification

According to the experience in $Mg[B(OR^F)_4]_2$, the fluorination strategy could improve the oxidative stability of anions to

Table 3. Property comparison of the Mg–Carborane Cluster electrolytes and their cathode compatibility.

Electrolyte	Ionic conductivity [mS cm^{-1}] (concentration)	Coulombic efficiency	Oxidative stability [V] (substrate)	Cathode	Capacity [mAh g^{-1}] @ current density [mA g^{-1}] (cycle)	Ref.
$[(C_2B_{10}H_{11})_2MgCl]^-[Mg_2Cl_3]^+$/THF	0.6 (100 mg mL^{-1})	98%	3.2 (Pt)	Mo_6S_8	90 @ 6 (30)	[39]
$Mg(CB_{11}H_{12})_2$/TG	1.8 (0.75 M)	99%	3.8 (Pt)	Mo_6S_8	80 @ 10 (10)	[77]
				a-MnO_2	90 @ 0.2[a] (10)	[77]
				PTO	265 @ 0.2 C[b] (700)	[78]
				P(NDI2OD-T2)	50.5 @ 0.5 C[c] (1)	[79]

[a] unit: mA cm^{-2}; [b] 1 C = 408 mA g^{-1}; [c] 1 C = 54 mA g^{-1}.

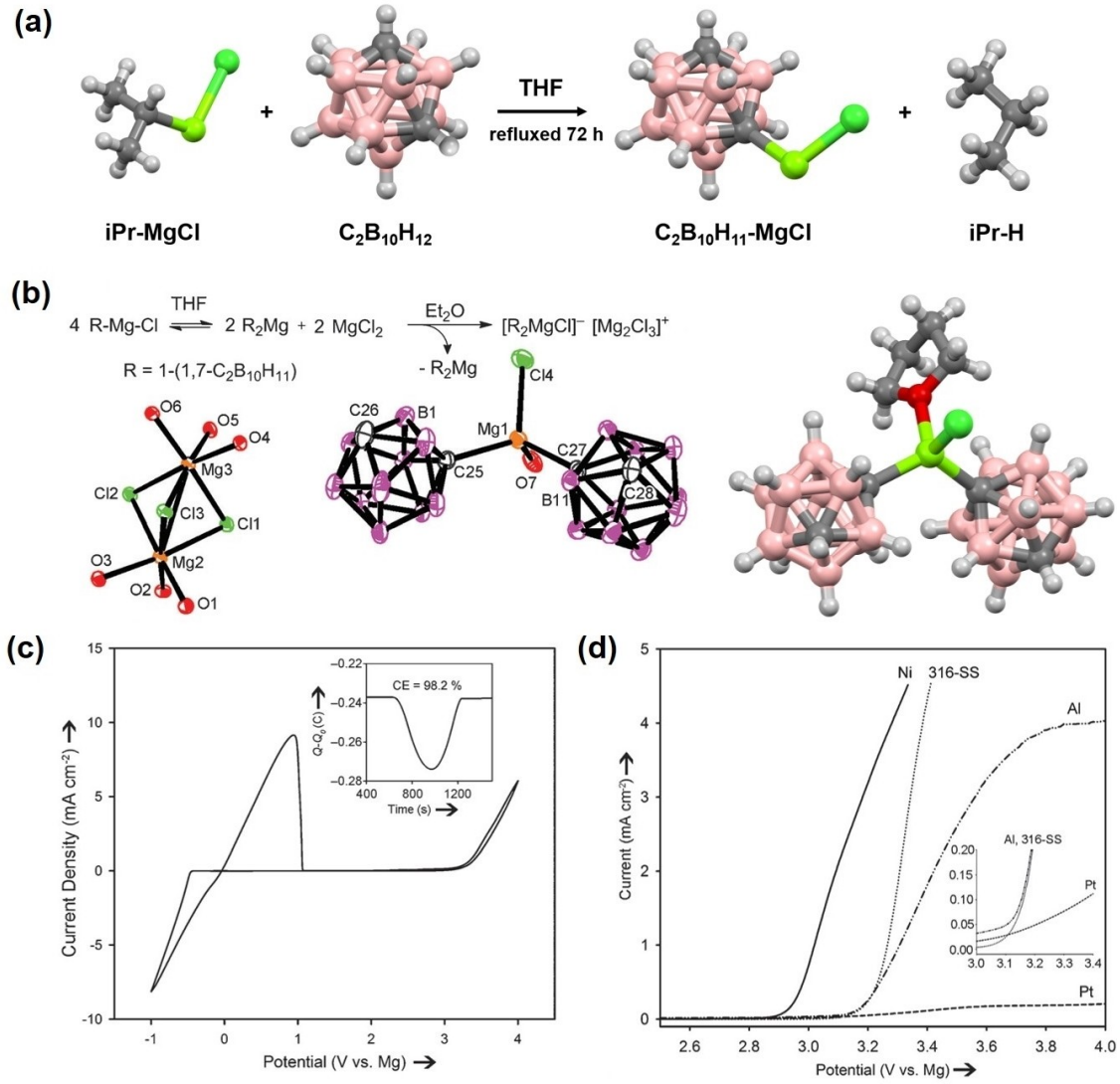

Figure 6. a) Synthetic route of the $C_2B_{10}H_{11}$–MgCl salt. b) Proposed mechanism for the formation of $[R_2MgCl]^-[Mg_2Cl_3]^+$ (top); X–ray single–crystal structure (bottom) and corresponding scheme (right) of the $[R_2MgCl]^-[Mg_2Cl_3]^+$. c) CV of the Mg plating/stripping and d) LSVs on Pt, SS, Ni, and Al electrodes using the $[R_2MgCl]^-[Mg_2Cl_3]^+$/THF electrolyte. b)–d) Reprinted from Ref. [39] with permission. Copyright (2014) Wiley–VCH.

some extent. Therefore, Zavadil et al. evaluated the impact of functionalization of the parent $[CB_{11}H_{12}]^-$ anion on its stability.[81] They reported that replacing the carbon-vertex proton with more electronegative fluorine or trifluoromethyl ligand could increase oxidative stability and reduce the contact-ion pair formation energy while maintaining reductive stability. The $[FCB_{11}H_{11}]^-$-based electrolyte (5 mM in G3 (triglyme)) presented a high CE (96%) and low overpotentials. As the ESP of $[FCB_{11}H_{11}]^-$ (right) and $[CB_{11}H_{12}]^-$ (left) shown in Figure 7(d), the boron antipodal to carbon, and the midpoint of the two adjacent borons bound to Mg^{2+} show withdrawal of electron density from the coordination site after fluorination. The binding energies of substitutional functional groups are shown in Figure 7(e), the Mg^{2+}-anion binding energy of electron-withdrawing groups (fluoro and trifluoromethyl) is generally lower than that of electron-donating groups (alkyl and amino), which means that the weak coordination effect is more prominent in the fluorination modification electrolytes. Kanazawa et al. furthered the exploration of this halogenation modification on the B-vertices (opposite to the C-vertex), they found that the Cl/Br functionalization of the lower hemisphere of the $[CB_{11}H_{12}]^-$ anion could significantly improve the solubility (1 M) and ionic conductivity (~6 mS cm^{-1}) without compromising redox stability.[82]

4.3. Anode–electrolyte interface

Through systematic electrochemical analyses and microscopic and spectroscopic characterizations, Guo et al. have demonstrated superior Mg plating–stripping performance of the $Mg(CB_{11}H_{12})_2$ electrolyte.[83] The relatively superior electrochemical performance of $Mg[CB_{11}H_{12}]_2$ could be attributed to its chemical and electrochemical stability at the Mg/electrolyte

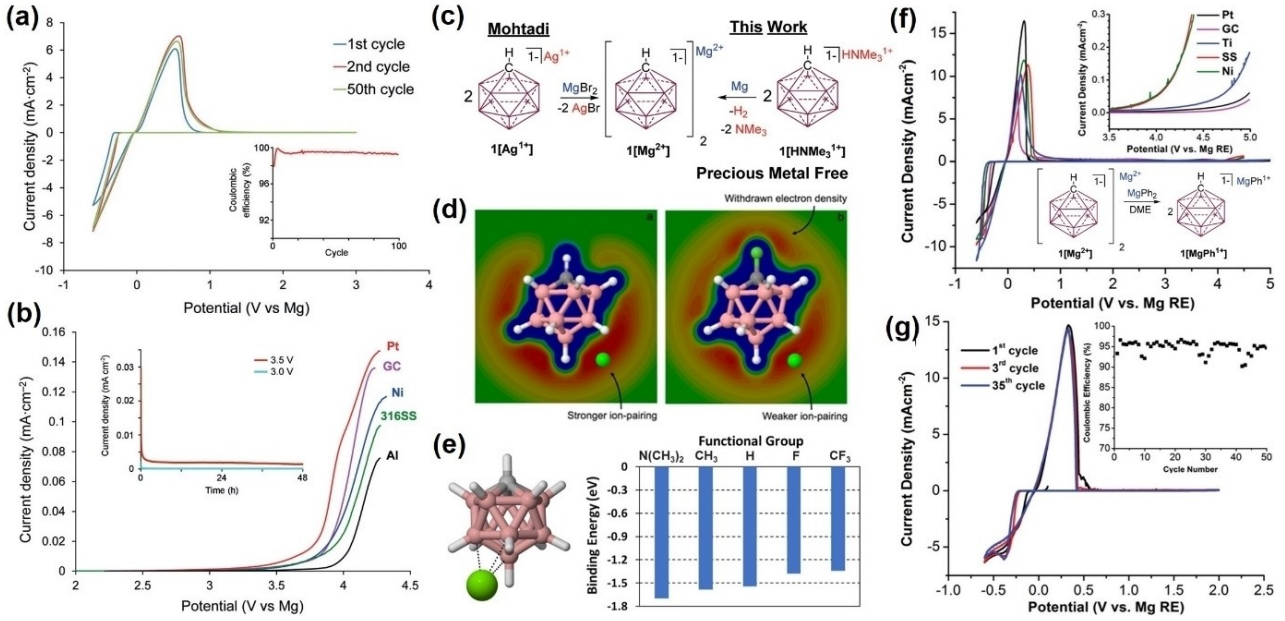

Figure 7. a) Selected CVs and Coulombic efficiency of the Mg deposition/stripping using 0.75 M $Mg(CB_{11}H_{12})_2$/TG electrolyte on Pt, 5 mV s^{-1}. b) LSVs and chronoamperometry (316SS disk electrodes) of the 0.75 M $Mg(CB_{11}H_{12})_2$/TG electrolyte on different electrodes, 5 mV s^{-1}. a) and b) Reprinted from Ref. [77] with permission. Copyright (2015) Wiley–VCH. c) Two routes to synthesize the $Mg(CB_{11}H_{12})_2$: Ag precursor (left) and Ag-free (right). d) Electrostatic potential imposed by the $[CB_{11}H_{12}]^-$/$[FCB_{11}H_{11}]^-$ anion in the plane of Mg^{2+}. e) Preferred (tridentate) coordination in Mg^{2+}–$[RCB_{11}H_{11}]^-$ ion pairs and corresponding cation/anion binding energy (eV). d) and e) Reprinted from Ref. [81] with permission. Copyright (2018) American Chemical Society. f) Initial CVs of the Mg deposition/stripping on various electrodes using the 0.4 M [MgPh·THF·2DME] $[CB_{11}H_{12}]$ electrolyte, 5 mV s^{-1}. g) Selected CVs and Coulombic efficiency of the Mg deposition/stripping on Pt, 5 mV s^{-1}. c), f), g) Reprinted from Ref. [80] with permission. Copyright (2015) Royal Society of Chemistry.

interface. From XPS and TEM analysis, Arthur et al. proposed that the SEI is amorphous and composed of carbon and boron species, but the SEI formation does not occur, when Mg-metal deposition and dissolution are diminished (e.g., under 0 °C and 10 mA cm^{-2} current density).[84]

5. Highlight and Rethink

5.1. Aluminium or boron?

As two adjacent chemical elements in group III A, the question of choosing B or Al as the central atom of anions is accompanied by the development of electrolytes for RMBs. In 2001, Aurbach et al. discovered that simply replacing the Lewis acid triphenylborane (BPh_3) with a stronger Lewis acid $AlCl_3$ resulted in an in situ generated electrolyte with higher voltage stabilities more than 600 mV.[44] Henceforth, Al^{3+} derivatives derived from $AlCl_3$ were widely used in magnesium electrolytes for a long time, and even once regarded as the key to the improvement of the reversibility of the anodic Mg plating/stripping. However, this simple and directing $AlCl_3$ adding strategy inevitably introduces corrosive Cl^-, which has been demonstrated an important role in depassivating magnesium anode, reducing the plating/stripping overpotential, and thus bringing significant superiority of early Al-based electrolytes. Based on recently B-centered WCAs electrolytes, the counterpart of the Al-centered anion also has aroused extensive research interest. Mandai et al. compared the electrochemical Mg plating/stripping performance in $[Al(Ohfip)_4]^-$ and $[B(Ohfip)_4]^-$ electrolytes under the same condition.[85] As shown in Figure 8(a–d), the $[Al(Ohfip)_4]^-$ exhibits similar overpotentials and CEs in the asymmetry Mg||Cu semi-cell compared with the $[B(Ohfip)_4]^-$, but the oxidation stability decreased slightly in LSVs. It is worth noting that this report observed an inactive response of $[Al(Ohfip)_4]^-$/G3. The Mg(Al–OFP)/THF was proposed by Cui et al., as shown in Figure 8(g), the HOMO energy of the $[Al–OFP]^-$ is lower than the $[B–OFP]^-$, which represented a more ideal oxidative stability.[86] In Figure 8(h), the higher LUMO energy of $[Al–OFP·THF]^-$ also proves its superior reductive stability than $[Al–OFP·DME]^-$, and the more difficult to be reduced/decomposed by metallic Mg.

5.2. Conditioning process?

The "conditioning" process was first proposed in the magnesium aluminum chloride complex (MACC) electrolyte whereby $MgCl_2$ and $AlCl_3$ are simply dissolved at a 2:1 mole ratio in THF.[17a,87] The most typical characteristic of this "conditioning" process is that the reversibility of Mg plating/stripping is extremely poor in initial electrochemical cycles, and the response current density increases significantly with the electrochemical cycles. The equilibria responsible for the active dimer $[Mg_2(\mu–Cl)_3·6THF]^+$ cation clusters are complicated and could be affected by various components, including solvents. Meanwhile, the presence of Cl^- is regarded as an important

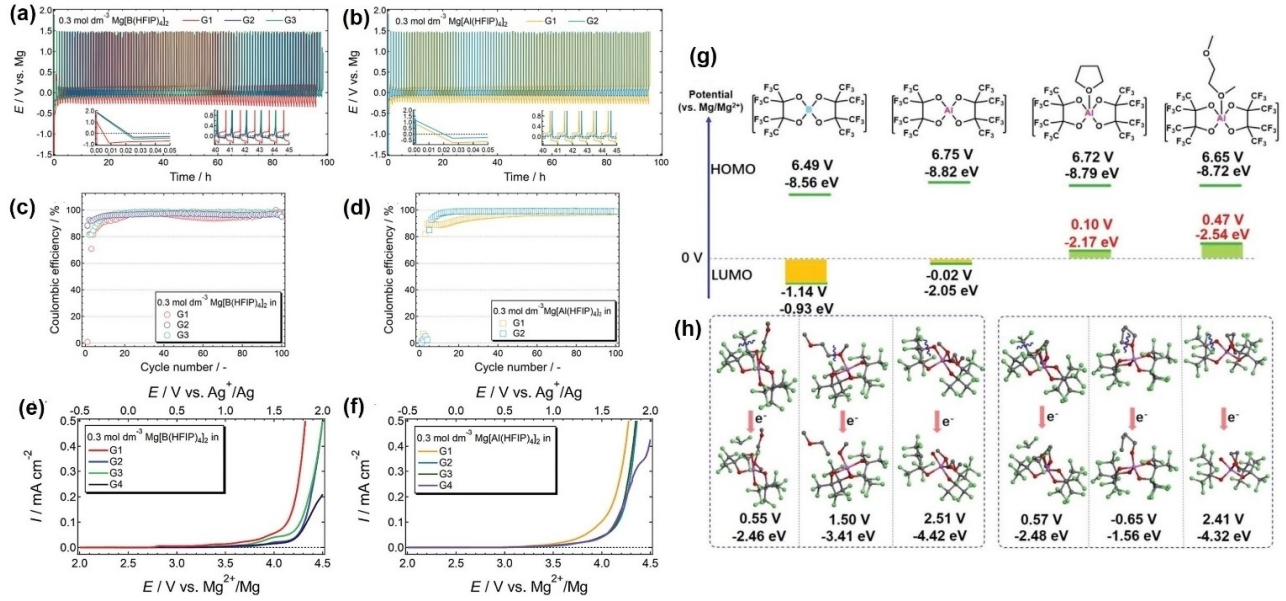

Figure 8. a), b) Galvanostatic Mg plating/stripping profiles and c), d) Coulombic efficiencies using 0.3 M $Mg[Z(Ohfip)_4]_2$ (Z=B, Al) electrolytes, 0.5 mA cm^{-2} on Cu. e), f) LSVs of the $Mg[Z(Ohfip)_4]_2$ electrolytes, 1 mV s^{-1} on Pt. a)–f) Reprinted from Ref. [85a]. Copyright (2021) The Author(s). Published by the Royal Society of Chemistry. g) Calculated HOMO/LUMO (potential *vs.* Mg^{2+}/Mg) of bare B–OFP, bare Al–OFP, THF and DME coordinated Al–FP. h) Calculated reduction decomposition potentials of Mg(Al–OFP)/DME (left) and Mg(Al–OFP)/THF (right) in different bond–breaking ways. g), h) Reprinted from Ref. [86] with permission. Copyright (2020) Wiley–VCH.

associator to depassivate the inert component on the Mg anode.

Although less pronounced than the MACC electrolyte, this electrochemical pre-activation phenomenon which is similar to the "conditioning" process still exists in advanced Mg–B electrolytes. As shown in Figure 9, the $Mg(CB_{11}H_{12})_2$/TG (Figure 9a–d), $Mg[B(Ohfip)_4]_2$/DME (Figure 9e, f), and MgF_2-$B(Ohfip)_3$/DME (Figure 9g–i) both showed an inadequate CE in the previous electrochemical cycles even after excluding the influence of impurities such as moisture, but the electrochemical performance was gradually improved in the subsequent cycles. Electrochemical impedance spectroscopy of the $Mg(CB_{11}H_{12})_2$ electrolyte demonstrated newly formed anode-electrolyte interfaces and the improvement upon each subsequent cycle.[88] Recently, more research tends to assume that the previous electrochemical activation process is still necessary for Mg–B electrolytes, that is, a certain number of electrochemical cycling is needed to achieve a stable CE of Mg plating/stripping.[89] Such similar "conditioning" or "activation" process is undoubtedly directly related to the formation and component of the Mg metal-electrolyte interface. Researches on the interaction between chloride-containing electrolytes and Mg metal anode suggest that the switchable interfacial behavior emerges from the adsorption of Cl^- anions at the Mg surface.[90,91] Therefore, in addition to the strategies of the Mg anode protective layer and activator additive mentioned above, exploring the specific formation mechanism of the anode-electrolyte layer is also crucial.

5.3. Solvent effect

Solvent has been widely proved to have a great effect on the electrochemical activity of metallic Mg anode. Early studies have generally concluded that magnesium batteries are highly solvent-reliant, namely, ethers are primarily regarded as the only solvent capable of supporting reversible Mg plating/stripping for their superior reduction stability. When replacing the DG solvent with acetonitrile, the Mg–B–OFP electrolyte manifested a non-reversible plating/stripping behavior.[46] Nevertheless, ethers also have their defects, such as inferior oxidation stability and typically much more volatile and flammable, which bring many difficulties to the design of the practical application and high voltage electrolytes. Therefore, numerous reports focused on the ether-cosolvent strategy by adding solvents with superior oxidative stability. Ionic liquids are a typical choice not only to increase the thermal stability but also greatly improves the ionic conductivity of the electrolyte. On the other hand, there are many reports demonstrating that some unconventional solvents (e.g., carbonates,[93] DMSO[94]) could also be applied under the premise of reasonable artificial anode protective layers or rearranged solvation sheath.[95]

6. Summary and Outlook

6.1. Summary

Boron-magnesium electrolytes with attractive comprehensive performance have become new trends and the most potential

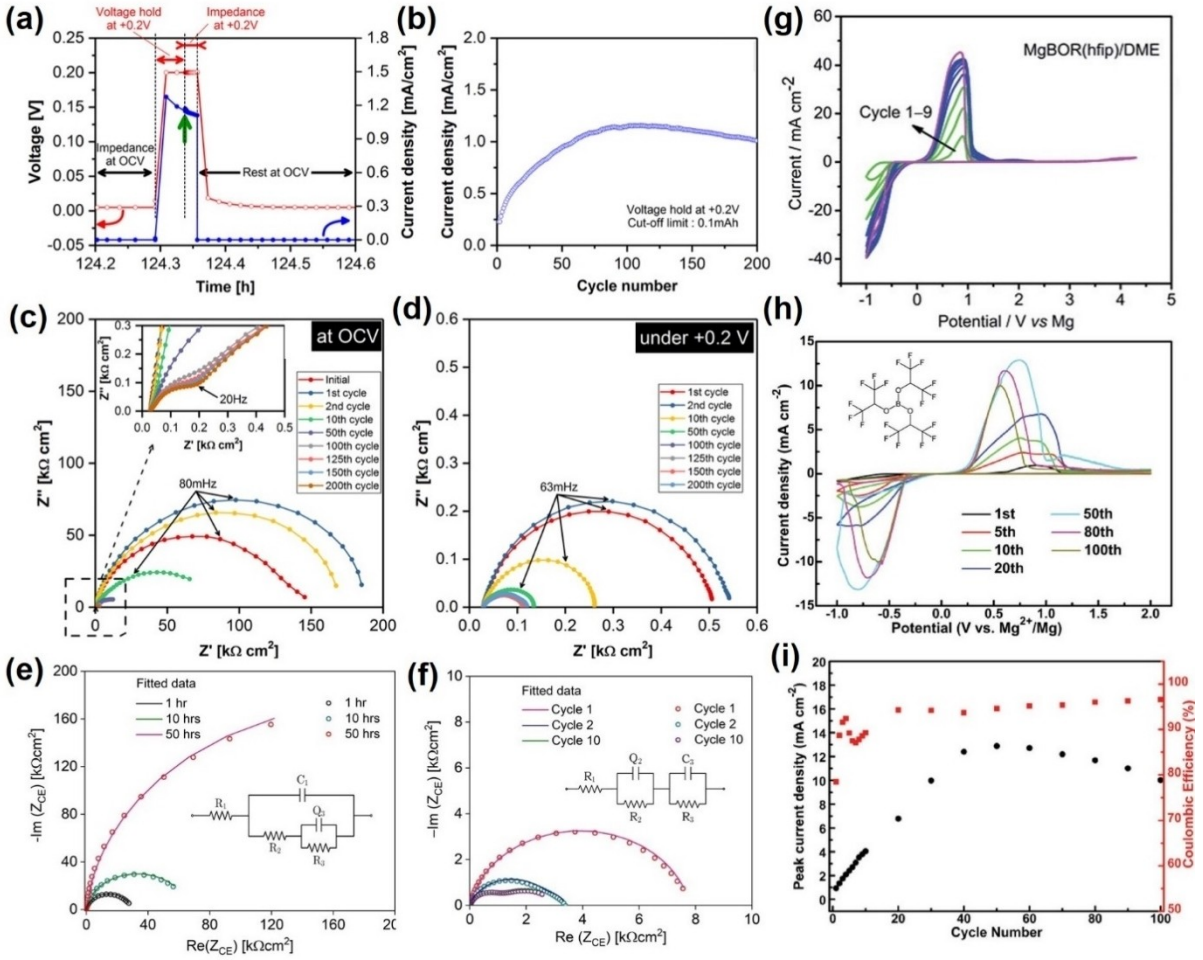

Figure 9. The $Mg(CB_{11}H_{12})_2$/TG electrolyte: a) Current/voltage responses for a symmetrical Mg||Mg cell; b) observed current densities at the end of each +0.2 V voltage hold and before impedance measurement at +0.2 V as a function of cycle number; c), d) Nyquist plots of the symmetrical Mg||Mg cell as a function of cycle number under OCV (open–circuit voltage) and +0.2 V bias, respectively. a)–d) Reprinted from Ref. [88] with permission. Copyright (2017) American Chemical Society. The $Mg[B(Ohfip)_4]_2$/DME electrolyte: Impedance spectra from the anode side of the e) pre–cycled and f) post–cycled three–electrode cell. e), f) Reprinted from Ref. [92] with permission. Copyright (2022) Wiley–VCH. g) Initial CVs of the Mg plating/stripping on Pt, 25 $mV s^{-1}$. Reprinted from Ref. [54b] with permission. Copyright (2017) Royal Society of Chemistry. The MgF_2–$B(Ohfip)_3$/DME electrolyte: h) CVs of the Mg stripping/plating on SS, 5 $mV s^{-1}$; i) peak current density during the Mg stripping process and the corresponding Coulombic efficiencies obtained from CV curves. h), i) Reprinted from Ref. [49] with permission. Copyright (2017) Wiley–VCH.

candidates in the research of RMBs, especially considering the rapid development and requirement of electrophilic (e.g., S, Se) and high-voltage (e.g., transition metal oxides) cathodes. In the family of halogen-free B-centered electrolytes, $Mg(BH_4)_2$ suffered from low oxidative stability and limited solubility. However, WCAs Mg–B electrolytes developed from the $[BH_4]^-$ have gradually become the protagonist in the R&D of high-performance Mg electrolytes.

During the process of practical applications of these high-performance Mg–B electrolytes, synthesis cost and accessibility are important issues that could not be ignored. As the cost comparison shown in Figure 10(a), after splitting the $Mg(BH_4)_2$ into cheaper and more readily available $Mg(Bu)_2$ and BH_3, the synthesis cost of the $Mg[B(Ohfip)_4]_2$ is decreased by 54% (Route I: 12,576 $ per mole; Route II: 5,820 $ per mole). Furthermore, the usage of lower fluorination tfe-OH reduces the cost by 78% totally. In the route of in-situ reaction (Figure 10b), the use of lower-fluorinated borates also reduces the cost by 70% (from 89 $/mmol to 27 $/mmol). As shown in Figure 10(c), the influence of the synthesis pathway change on the key features of electrolytes is multi-dimensional and comprehensive. Albeit with a complicated synthetic procedure and high raw material price, magnesium fluoroalkoxyborate and carbaborate originating from $Mg(BH_4)_2$ have the most ideal electrochemical performance and are favorably adapted to common cathodes at the moment. Under the premise of acceptable electrochemical performance, low fluorination strategy (lower cost) and in-situ reaction synthesis (better accessibility) are possibly two key factors to achieve practical Mg–B electrolytes in the future.

6.2. Outlook

Given the facing challenges of Mg–B electrolytes and the case studies of emerging topics, the following directions are

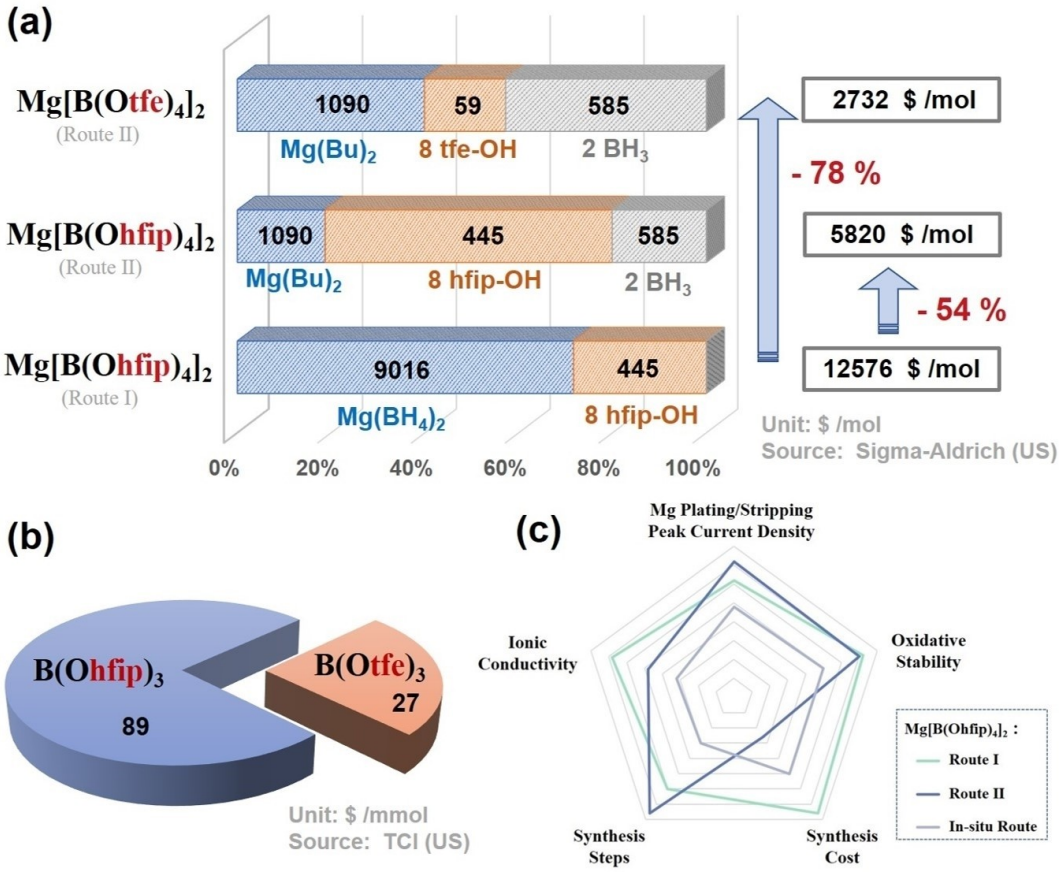

Figure 10. a) Cost calculation of three synthesis routes for the $Mg[B(Ohfip)_4]_2$ and $Mg[B(Otfe)_4]_2$ electrolytes. b) mmol cost of $B(Ohfip)_3$ and $B(Otfe)_3$ borates. Chemical price information is fresh collected from the Sigma-Aldrich (US) and TCI (US), respectively. c) Key features of three different routes to synthesize the $Mg[B(Ohfip)_4]_2$ electrolyte.

promising and need a deeper comprehension in the future research: 1) reasonable additive design; 2) solvation structure optimization; 3) Mg anode/cathode–electrolyte interface. Meanwhile, more advanced monitoring techniques, such as electrochemistry-related operando characterizations and high-energy synchrotron X-ray, will continue to play a key role in investigating the chemical phase distribution of SEI, multi-scale imaging, and the interface evolution during the charge/discharge process, and finally promoting the overall understanding of Mg–B electrolytes.

Acknowledgements

We acknowledge the financial support from the National Natural Science Foundation of China (No. 21975159, 2157316) and Oceanic Interdisciplinary Program of Shanghai Jiao Tong University (No. WH410260401/006).

Conflict of Interest

The authors declare no conflict of interest.

Keywords: boron · electrolytes · magnesium · rechargeable magnesium batteries · weakly coordinator anion

[1] a) M. Armand, J. Tarascon, *Nature* **2008**, *451*, 652–657; b) B. Dunn, H. Kamath, J. Tarascon, *Science* **2011**, *334*, 928–935.
[2] a) M. Li, J. Lu, Z. Chen, K. Amine, *Adv. Mater.* **2018**, *30*, 1800561; b) Y. Liu, Y. Zhu, Y. Cui, *Nat. Energy* **2019**, *4*, 540–550; c) J. Choi, D. Aurbach, *Nat. Rev. Mater.* **2016**, *1*, 16013.
[3] a) J. Zhang, Z. Chang, Z. Zhang, A. Du, S. Dong, Z. Li, G. Li, G. Cui, *ACS Nano* **2021**, *15*, 15594–15624; b) X. Lei, X. Liang, R. Yang, F. Zhang, C. Wang, C. Lee, Y. Tang, *Small* **2022**, *18*, 2200418; c) Y. Lu, C. Wang, Q. Liu, X. Li, X. Zhao, Z. Guo, *Small Methods* **2021**, *5*, 2001303.
[4] M. Guo, C. Yuan, T. Zhang, X. Yu, *Small* **2022**, *18*, 2106981.
[5] J. Kwak, Y. Jeoun, S. Oh, S. Yu, J. Lim, Y. Sung, S. Yu, H. Lim, *ACS Energy Lett.* **2022**, *7*, 162–170.
[6] R. Davidson, A. Verma, D. Santos, F. Hao, C. Fincher, S. Xiang, J. Van Buskirk, K. Xie, M. Pharr, P. Mukherjee, S. Banerjee, *ACS Energy Lett.* **2019**, *4*, 375–376.
[7] R. Davidson, A. Verma, D. Santos, F. Hao, C. Fincher, D. Zhao, V. Attari, P. Schofield, J. Van Buskirk, A. Fraticelli-Cartagena, T. Alivio, R. Arroyave, K. Xie, M. Pharr, P. Mukherjee, S. Banerjee, *Mater. Horiz.* **2020**, *7*, 843–854.
[8] M. Jackle, K. Helmbrecht, M. Smits, D. Stottmeister, A. Gross, *Energy Environ. Sci.* **2018**, *11*, 3400–3407.
[9] a) Z. Lu, A. Schechter, M. Moshkovich, D. Aurbach, *J. Electroanal. Chem.* **1999**, *466*, 203–217; b) L. Lossius, F. Emmenegger, *Electrochim. Acta* **1996**, *41*, 445–447; c) A. Lautar, J. Bitenc, T. Rejec, R. Dominko, J. Filhol, M. Doublet, *J. Am. Chem. Soc.* **2020**, *142*, 5146–5153.
[10] T. Gregory, R. Hoffman, R. Winterton, *J. Electrochem. Soc.* **1990**, *137*, 775–780.

[11] a) Y. Gofer, O. Chusid, H. Gizbar, Y. Viestfrid, H. Gottlieb, V. Marks, D. Aurbach, *Electrochem. Solid-State Lett.* **2006**, *9*, A257; b) D. Aurbach, Z. Lu, A. Schechter, Y. Gofer, H. Gizbar, R. Turgeman, Y. Cohen, M. Moshkovich, E. Levi, *Nature* **2000**, *407*, 724–727.
[12] O. Mizrahi, N. Amir, E. Pollak, O. Chusid, V. Marks, H. Gottlieb, L. Larush, E. Zinigrad, D. Aurbach, *J. Electrochem. Soc.* **2008**, *155*, A103–A109.
[13] a) H. Yoo, I. Shterenberg, Y. Gofer, G. Gershinsky, N. Pour, D. Aurbach, *Energy Environ. Sci.* **2013**, *6*, 2265–2279; b) N. Pour, Y. Gofer, D. Major, D. Aurbach, *J. Am. Chem. Soc.* **2011**, *133*, 6270–6278.
[14] a) H. Kim, T. Arthur, G. Allred, J. Zajicek, J. Newman, A. Rodnyansky, A. Oliver, W. Boggess, J. Muldoon, *Nat. Commun.* **2011**, *2*, 427; b) Z. Zhao-Karger, X. Zhao, D. Wang, T. Diemant, R. Behm, M. Fichtner, *Adv. Energy Mater.* **2015**, *5*, 1401155; c) B. Vinayan, Z. Zhao-Karger, T. Diemant, V. Chakravadhanula, N. Schwarzburger, M. Cambaz, R. Behm, C. Kubel, M. Fichtner, *Nanoscale* **2016**, *8*, 3296–3306.
[15] T. Gao, X. Ji, S. Hou, X. Fan, X. Li, C. Yang, F. Han, F. Wang, J. Jiang, K. Xu, C. Wang, *Adv. Mater.* **2018**, *30*, 1704313.
[16] a) D. Huang, S. Tan, M. Li, D. Wang, C. Han, Q. An, L. Mai, *ACS Appl. Mater. Interfaces* **2020**, *12*, 17474–17480; b) Y. Yang, W. Wang, Y. NuLi, J. Yang, J. Wang, *ACS Appl. Mater. Interfaces* **2019**, *11*, 9062–9072.
[17] a) K. See, K. Chapman, L. Zhu, K. Wiaderek, O. Borkiewicz, C. Barile, P. Chupas, A. Gewirth, *J. Am. Chem. Soc.* **2016**, *138*, 328–337; b) T. Liu, Y. Shao, G. Li, M. Gu, J. Hu, S. Xu, Z. Nie, X. Chen, C. Wang, J. Liu, *J. Mater. Chem. A* **2014**, *2*, 3430–3438.
[18] a) R. Horia, D. Nguyen, A. Eng, Z. Seh, *Batteries & Supercaps* **2022**, *5*, e202200011; b) R. Attias, M. Salama, B. Hirsch, Y. Goffer, D. Aurbach, *Joule* **2019**, *3*, 27–52.
[19] P. Bonnick, J. Muldoon, *Adv. Funct. Mater.* **2020**, *30*, 1910510.
[20] S. Hou, X. Ji, K. Gaskell, P. Wang, L. Wang, J. Xu, R. Sun, O. Borodin, C. Wang, *Science* **2021**, *374*, 172–178.
[21] J. Muldoon, C. Bucur, A. Oliver, J. Zajicek, G. Allred, W. Boggess, *Energy Environ. Sci.* **2013**, *6*, 482–487.
[22] Y. Guo, F. Zhang, J. Yang, F. Wang, Y. NuLi, S. Hirano, *Energy Environ. Sci.* **2012**, *5*, 9100–9106.
[23] Y. Liang, H. Dong, D. Aurbach, Y. Yao, *Nat. Energy* **2020**, *5*, 646–656.
[24] a) H. Li, K. Kikuchi, Y. Nakamori, N. Ohba, K. Miwa, S. Towata, S. Orimo, *Acta Mater.* **2008**, *56*, 1342–1347; b) H. Li, Y. Yan, S. Orimo, A. Zuttel, C. Jensen, *Energies* **2011**, *4*, 185–214.
[25] J. Connor, W. Reid, G. Wood, *J. Electrochem. Soc.* **1957**, *104*, 38–41.
[26] a) D. Samuel, C. Steinhauser, J. Smith, A. Kaufman, M. Radin, J. Naruse, H. Hiramatsu, D. Siegel, *ACS Appl. Mater. Interfaces* **2017**, *9*, 43755–43766; b) H. Xu, Z. Zhang, J. Li, L. Qiao, C. Lu, K. Tang, S. Dong, J. Ma, Y. Liu, X. Zhou, G. Cui, *ACS Appl. Mater. Interfaces* **2018**, *10*, 23757–23765.
[27] R. Mohtadi, M. Matsui, T. Arthur, S. Hwang, *Angew. Chem. Int. Ed.* **2012**, *51*, 9780–9783; *Angew. Chem.* **2012**, *124*, 9918–9921.
[28] Y. Shao, T. Liu, G. Li, M. Gu, Z. Nie, M. Engelhard, J. Xiao, D. Lv, C. Wang, J. Zhang, J. Liu, *Sci. Rep.* **2013**, *3*, 3130.
[29] F. Tuerxun, Y. Abulizi, Y. NuLi, S. Su, J. Yang, J. Wang, *J. Power Sources* **2015**, *276*, 255–261.
[30] S. Su, Y. NuLi, N. Wang, D. Yusipu, J. Yang, J. Wang, *J. Electrochem. Soc.* **2016**, *163*, D682–D688.
[31] H. Wang, J. Ryu, Y. Shao, V. Murugesan, K. Persson, K. Zavadil, K. Mueller, J. Liu, *ChemElectroChem* **2021**, *8*, 3013–3029.
[32] Z. Ma, M. Kar, C. Xiao, M. Forsyth, D. MacFarlane, *Electrochem. Commun.* **2017**, *78*, 29–32.
[33] R. Horia, D. Nguyen, A. Eng, Z. Seh, *Nano Lett.* **2021**, *21*, 8220–8228.
[34] Z. Li, T. Diemant, Z. Meng, Y. Xiu, A. Reupert, L. Wang, M. Fichtner, Z. Zhao-Karger, *ACS Appl. Mater. Interfaces* **2021**, *13*, 33123–33132.
[35] H. Wang, X. Feng, Y. Chen, Y. Liu, K. Han, M. Zhou, M. Engelhard, V. Murugesan, R. Assary, T. Liu, W. Henderson, Z. Nie, M. Gu, J. Xiao, C. Wang, K. Persson, D. Mei, J. Zhang, K. Mueller, J. Guo, K. Zavadil, Y. Y. Shao, J. Liu, *ACS Energy Lett.* **2020**, *5*, 200–206.
[36] T. Arthur, P. Glans, N. Singh, O. Tutusaus, K. Nie, Y. Liu, F. Mizuno, J. Guo, D. Alsem, N. Salmon, R. Mohtadi, *Chem. Mater.* **2017**, *29*, 7183–7188.
[37] N. Rajput, X. Qu, N. Sa, A. Burrell, K. Persson, *J. Am. Chem. Soc.* **2015**, *137*, 3411–3420.
[38] S. Strauss, *Chem. Rev.* **1993**, *93*, 927–942.
[39] T. Carter, R. Mohtadi, T. Arthur, F. Mizuno, R. Zhang, S. Shirai, J. Kampf, *Angew. Chem. Int. Ed.* **2014**, *53*, 3173–3177; *Angew. Chem.* **2014**, *126*, 3237–3241.
[40] Y. Shao, N. Rajput, J. Hu, M. Hu, T. Liu, Z. Wei, M. Gu, X. Deng, S. Xu, K. Han, J. Wang, Z. Nie, G. Li, K. Zavadil, J. Xiao, C. Wang, W. Henderson, J. Zhang, Y. Wang, K. Mueller, K. Persson, J. Liu, *Nano Energy* **2015**, *12*, 750–759.
[41] T. Watkins, A. Kumar, D. Buttry, *J. Am. Chem. Soc.* **2016**, *138*, 641–650.
[42] C. Liebenow, Z. Yang, P. Lobitz, *Electrochem. Commun.* **2000**, *2*, 641–645.
[43] J. Zhu, Y. Guo, J. Yang, Y. NuLi, F. Zhang, J. Wang, S. Hirano, *J. Power Sources* **2014**, *248*, 690–694.
[44] D. Aurbach, H. Gizbar, A. Schechter, O. Chusid, H. Gottlieb, Y. Gofer, I. Goldberg, *J. Electrochem. Soc.* **2001**, *149*, A115–A121.
[45] a) J. Muldoon, C. Bucur, T. Gregory, *Chem. Rev.* **2014**, *114*, 11683–11720; b) H. Shuai, J. Xu, K. Huang, *Coord. Chem. Rev.* **2020**, *422*, 213478.
[46] J. Luo, Y. Bi, L. Zhang, X. Zhang, T. Liu, *Angew. Chem. Int. Ed.* **2019**, *58*, 6967–6971; *Angew. Chem.* **2019**, *131*, 7041–7045.
[47] T. Mandai, *ACS Appl. Mater. Interfaces* **2020**, *12*, 39135–39144.
[48] A. Du, Z. Zhang, H. Qu, Z. Cui, L. Qiao, L. Wang, J. Chai, T. Lu, S. Dong, T. Dong, H. Xu, X. Zhou, G. Cui, *Energy Environ. Sci.* **2017**, *10*, 2616–2625.
[49] Z. Zhang, Z. Cui, L. Qiao, J. Guan, H. Xu, X. Wang, P. Hu, H. Du, S. Li, X. Zhou, S. Dong, Z. Liu, G. Cui, L. Chen, *Adv. Energy Mater.* **2017**, *7*, 1602055.
[50] H. Xu, Z. Zhang, Z. Cui, A. Du, C. Lu, S. Dong, J. Ma, X. Zhou, G. Cui, *Electrochem. Commun.* **2017**, *83*, 72–76.
[51] W. Ren, D. Wu, Y. NuLi, D. Zhang, Y. Yang, Y. Wang, J. Yang, J. Wang, *ACS Energy Lett.* **2021**, *6*, 3212–3220.
[52] X. Huang, J. Wen, J. Lei, G. Huang, F. Pan, L. Li, *ACS Appl. Mater. Interfaces* **2022**, *14*, 8906–8915.
[53] M. Cheng, W. Ren, D. Zhang, S. Zhang, Y. Yang, X. Lv, J. Yang, J. Wang, Y. NuLi, *Energy Storage Mater.* **2022**, *51*, 764–776.
[54] a) K. Tang, A. Du, S. Dong, Z. Cui, X. Liu, C. Lu, J. Zhao, X. Zhou, G. Cui, *Adv. Mater.* **2020**, *32*, e1904987; b) Z. Zhao-Karger, M. Bardaji, O. Fuhr, M. Fichtner, *J. Mater. Chem. A* **2017**, *5*, 10815–10820.
[55] a) R. Lv, X. Guan, J. Zhang, Y. Xia, J. Luo, *Natl. Sci. Rev.* **2020**, *7*, 333–341; b) J. Zhang, X. Guan, R. Lv, D. Wang, P. Liu, J. Luo, *Energy Storage Mater.* **2020**, *26*, 408–413.
[56] Z. Meng, Z. Li, L. Wang, T. Diemant, D. Bosubabu, Y. Tang, R. Berthelot, Z. Zhao-Karger, M. Fichtner, *ACS Appl. Mater. Interfaces* **2021**, *13*, 37044–37051.
[57] V. Parambath, Z. Zhao-Karger, T. Diemant, M. Jackle, Z. Li, T. Scherer, A. Gross, R. Behm, M. Fichtner, *J. Mater. Chem. A* **2020**, *8*, 22998–23010.
[58] P. Jankowski, Z. Li, Z. Zhao-Karger, T. Diemant, M. Fichtner, T. Vegge, J. Lastra, *Energy Storage Mater.* **2022**, *45*, 1133–1143.
[59] J. Drews, P. Jankowski, J. Hacker, Z. Li, T. Danner, J. Lastra, T. Vegge, N. Wagner, K. Friedrich, Z. Zhao-Karger, M. Fichtner, A. Latz, *ChemSusChem* **2021**, *14*, 4820–4835.
[60] Z. Zhao-Karger, R. Liu, W. Dai, Z. Li, T. Diemant, B. Vinayan, C. Minella, X. Yu, A. Manthiram, R. Behm, M. Ruben, M. Fichtner, *ACS Energy Lett.* **2018**, *3*, 2005–2013.
[61] R. Mohtadi, *Molecules* **2020**, *25*, 1791.
[62] a) R. King, *Chem. Rev.* **2001**, *101*, 1119–1152; b) Z. Chen, R. King, *Chem. Rev.* **2005**, *105*, 3613–3642.
[63] a) S. Korbe, P. Schreiber, J. Michl, *Chem. Rev.* **2006**, *106*, 5208–5249; b) L. Toom, A. Kutt, I. Leito, *Dalton Trans.* **2019**, *48*, 7499–7502.
[64] B. Vinayan, H. Euchner, Z. Zhao-Karger, M. Cambaz, Z. Li, T. Diemant, R. Behm, A. Gross, M. Fichtner, *J. Mater. Chem. A* **2019**, *7*, 25490–25502.
[65] H. Kaland, F. Fagerli, J. Jacobsen, Z. Zhao-Karger, M. Fichtner, K. Wiik, N. Wagner, *ChemSusChem* **2021**, *14*, 1864–1873.
[66] Z. Li, B. Vinayan, P. Jankowski, C. Njel, A. Roy, T. Vegge, J. Maibach, J. G. Lastra, M. Fichtner, Z. Zhao-Karger, *Angew. Chem. Int. Ed.* **2020**, *59*, 11483–11490; *Angew. Chem.* **2020**, *132*, 11580–11587.
[67] A. Roy, V. Parambath, T. Diemant, G. Neusser, C. Kranz, R. Behm, Z. Li, Z. Zhao-Karger, M. Fichtner, *Batteries & Supercaps* **2022**, *5*, e202100305.
[68] Y. Shen, Y. Wang, Y. Miao, M. Yang, X. Zhao, X. Shen, *Adv. Mater.* **2020**, *32*, e1905524.
[69] Y. Xiu, Z. Li, V. Parambath, Z. Ding, L. Wang, A. Reupert, M. Fichtner, Z. Zhao-Karger, *Batteries & Supercaps* **2021**, *4*, 1850–1857.
[70] E. Abouzari-Lotf, R. Azmi, Z. Li, S. Shakouri, Z. Chen, Z. Zhao-Karger, S. Klyatskaya, J. Maibach, M. Ruben, M. Fichtner, *ChemSusChem* **2021**, *14*, 1840–1846.
[71] Z. Zhang, B. Chen, H. Xu, Z. Cui, S. Dong, A. Du, J. Ma, Q. Wang, X. Zhou, G. Cui, *Adv. Funct. Mater.* **2018**, *28*, 1701718.
[72] X. Qu, A. Du, T. Wang, Q. Kong, G. Chen, Z. Zhang, J. Zhao, X. Liu, X. Zhou, S. Dong, G. Cui, *Angew. Chem. Int. Ed.* **2022**, *61*, e202204423.
[73] X. Cheng, Z. Zhang, Q. Kong, Q. Zhang, T. Wang, S. Dong, L. Gu, X. Wang, J. Ma, P. Han, H. J. Lin, C. T. Chen, G. Cui, *Angew. Chem. Int. Ed.* **2020**, *59*, 11477–11482; *Angew. Chem.* **2020**, *132*, 11574–11579.
[74] T. Lu, Z. Zhang, B. Chen, S. Dong, C. Wang, A. Du, L. Wang, J. Ma, G. Cui, *Mater. Today* **2020**, *17*, 100450.

[75] A. Du, Y. Zhao, Z. Zhang, S. Dong, Z. Cui, K. Tang, C. Lu, P. Han, X. Zhou, G. Cui, *Energy Storage Mater.* **2020**, *26*, 23–31.
[76] T. Pavcnik, J. Bitenc, K. Pirnat, R. Dominko, *Batteries & Supercaps* **2021**, *4*, 815–822.
[77] O. Tutusaus, R. Mohtadi, T. Arthur, F. Mizuno, E. Nelson, Y. Sevryugina, *Angew. Chem. Int. Ed.* **2015**, *54*, 7900–7904; *Angew. Chem.* **2015**, *127*, 8011–8015.
[78] H. Dong, O. Tutusaus, Y. Liang, Y. Zhang, Z. Lebens-Higgins, W. Yang, R. Mohtadi, Y. Yao, *Nat. Energy* **2020**, *5*, 1043–1050.
[79] H. Dong, Y. Liang, O. Tutusaus, R. Mohtadi, Y. Zhang, F. Hao, Y. Yao, *Joule* **2019**, *3*, 782–793.
[80] S. McArthur, L. Geng, J. Guo, V. Lavallo, *Inorg. Chem. Front.* **2015**, *2*, 1101–1104.
[81] N. Hahn, T. Seguin, K. Lau, C. Liao, B. Ingram, K. Persson, K. Zavadil, *J. Am. Chem. Soc.* **2018**, *140*, 11076–11084.
[82] M. Watanabe, J. Kanazawa, T. Hamamura, T. Shimokawa, K. Miyamoto, M. Hibisno, K. Nakura, Y. Inatomi, Y. Kitazawa, M. Uchiyama, *Mater. Adv.* **2021**, *2*, 937–941.
[83] R. Jay, A. W. Tomich, J. Zhang, Y. Zhao, A. De Gorostiza, V. Lavallo, J. Guo, *ACS Appl. Mater. Interfaces* **2019**, *11*, 11414–11420.
[84] N. Singh, T. Arthur, O. Tutusaus, J. Li, K. Kisslinger, H. Xin, E. Stach, X. Fan, R. Mohtadi, *ACS Appl. Energ. Mater.* **2018**, *1*, 4651–4661.
[85] a) T. Mandai, Y. Youn, Y. Tateyama, *Mater. Adv.* **2021**, *2*, 6283–6296; b) T. Pavčnik, M. Lozinšek, K. Pirnat, A. Vizintin, T. Mandai, D. Aurbach, R. Dominko, J. Bitenc, *ACS Appl. Mater. Interfaces* **2022**, *14*, 26766–26774.
[86] K. Tang, A. Du, X. Du, S. Dong, C. Lu, Z. Cui, L. Li, G. Ding, F. Chen, X. Zhou, G. Cui, *Small* **2020**, *16*, e2005424.
[87] a) C. Barile, E. Barile, K. Zavadil, R. Nuzzo, A. Gewirth, *J. Phys. Chem. C* **2014**, *118*, 27623–27630; b) R. Doe, R. Han, J. Hwang, A. Gmitter, I. Shterenberg, H. Yoo, N. Pour, D. Aurbach, *Chem. Commun.* **2014**, *50*, 243–245; c) T. Liu, Y. Shao, G. Li, M. Gu, J. Hu, S. Xu, Z. Nie, X. Chen, C. Wang, J. Liu, *J. Mater. Chem. A* **2014**, *2*, 3430–3438.
[88] O. Tutusaus, R. Mohtadi, N. Singh, T. Arthur, F. Mizuno, *ACS Energy Lett.* **2017**, *2*, 224–229.
[89] B. Dlugatch, M. Mohankumar, R. Attias, B. Krishna, Y. Elias, Y. Gofer, D. Zitoun, D. Aurbach, *ACS Appl. Mater. Interfaces* **2021**, *13*, 54894–54905.
[90] a) P. Canepa, G. Gautam, R. Malik, S. Jayaraman, Z. Rong, K. Zavadil, K. Persson, G. Ceder, *Chem. Mater.* **2015**, *27*, 3317–3325; b) P. Canepa, S. Jayaraman, L. Cheng, N. Rajput, W. Richards, G. Gautam, L. Curtiss, K. Persson, G. Ceder, *Energy Environ. Sci.* **2015**, *8*, 3718–3730; c) J. Ha, B. Adams, J. Cho, V. Duffort, J. Kim, K. Chung, B. Cho, L. Nazar, S. Oh, *J. Mater. Chem. A* **2016**, *4*, 7160–7164.
[91] R. Mohtadi, F. Mizuno, Beilstein *J. Nanobiotechnol.* **2014**, *5*, 1291–1311.
[92] A. Roy, V. Parambath, T. Diemant, G. Neusser, C. Kranz, R. Behm, Z. Li, Z. Zhao-Karger, M. Fichtner, *Batteries & Supercaps* **2022**, *5*, e202100305.
[93] C. Wang, Y. Huang, Y. Lu, H. Pan, B. B. Xu, W. Sun, M. Yan, Y. Jiang, *Nano-Micro Lett.* **2021**, *13*, 195.
[94] Q. Zou, Y. Sun, Z. Liang, W. Wang, Y. Lu, *Adv. Energy Mater.* **2021**, *11*, 2101552.
[95] Y. Li, P. Zuo, R. Li, H. Huo, Y. Ma, C. Du, Y. Gao, G. Yin, R. Weatherup, *ACS Appl. Mater. Interfaces* **2021**, *13*, 24565–24574.

Manuscript received: June 11, 2022
Revised manuscript received: July 25, 2022
Accepted manuscript online: July 27, 2022
Version of record online: August 18, 2022